Phys Chem Minerals (2000) 27: 398–418

ORIGINAL PAPER

A. Bosenick · M. T. Dove · C. A. Geiger

Simulation studies on the pyrope-grossular garnet solid solution

Received: 13 August 1999 / Revised, accepted: 10 December 1999

Abstract The local structural response of Ca/Mg substitution and the energetic effects associated with dodecahedral ordering in the pyrope-grossular garnet solid solution are derived from a combination of static lattice energy calculations and Monte Carlo simulations. We start with a thorough analysis of the goodness of the empirical potential models used for the modelling of aluminosilicate garnets. The degree of polyhedral distortion was found to be a sensitive indicator for the quality of the model and, by comparison with experimental data, was used to select the best of several available empirical potentials. The Ca/Mg substitution on the dodecahedral site in garnet was found to produce strong local distortions in the surrounding tetrahedral and octahedral polyhedra. This arises from the absence of rigid unit modes (RUMS) in the garnet structure, because local rotations of otherwise rigid SiO_4 tetrahedra and AlO_6 octahedra cannot occur in order to accommodate different-sized divalent cations in the dodecahedral sites. Strain effects, therefore, mainly govern the dodecahedral substitution, and the corresponding strain field around a dodecahedral site has a minimum radius of 5 Å. Pyrope-grossular solid solution compositions were modelled using a supercell approach. For several garnet compositions many different configurations representing individual disordered arrangements were relaxed. The resulting energies were analyzed in terms of different-neighbour interactions to determine the parameters of a model Hamiltonian. The corresponding interaction energies were found to be virtually independent of composition. Surprisingly, the nearest-neighbour interaction between edge-sharing dodecahedra is of no particular significance in the garnets. Instead, the strongest interaction is only via the third-nearest neighbours, i.e. dodecahedra that are edge-shared to a common SiO_4 tetrahedron. This cannot lead to dodecahedral long-range order in garnets, but can produce significant amounts of short-range order. Monte Carlo simulations were performed on several compositions to determine the macroscopic effects such as NMR-based cluster occupancy, ordering energy and configurational entropy of the short-range ordering process. As expected, the samples tend to random disorder at high temperatures, and at low temperatures it is compositions nearer Py50Gr50 that depart most strongly from random mixing. For example, a maximum reduction of 3.5 J mol^{-1} K^{-1} is predicted for Py75Gr25 and ~10 J mol^{-1} K^{-1} for Py50Gr50. A comparison of NMR cluster occupancy with experimental ^{29}Si MAS NMR resonance intensity is partly successful. However, the changes in NMR cluster occupancy are relatively low (~5%) compared to changes in configurational entropy (~30%), implying that it might be difficult to estimate exact entropy data from ^{29}Si MAS NMR line intensities.

Key words Garnet solid solution · Simulation studies · Short-range order · Thermodynamic integration

A. Bosenick · M. T. Dove (✉)
Department of Earth Sciences,
University of Cambridge,
Downing Street, Cambridge CB2 BEQ, UK
e-mail: martin@esc.cam.ac.uk
Tel.: +44-(0)1223-333482
Fax: +44-(0)1223-333450

C. A. Geiger
Institut für Geowissenschaften
der Christian-Albrechts-Universität zu Kiel,
Olshausenstr. 40, 24098 Kiel, Germany

Introduction

Being common constituents of the Earth's crust, upper mantle and transition zone, garnets are involved in many mineralogical phase equilibria which are used to unravel the P,T history of rocks. With few exceptions, natural garnets are compositionally complex multicomponent solid solutions. For crustal garnets, their chemical complexity can be described to a large extent in the quaternary aluminosilicate garnet system ($X_3Al_2Si_3O_{12}$,

X = Mg, Fe^{2+}, Ca, Mn^{2+}) consisting of the end-members pyrope, $Mg_3Al_2Si_3O_{12}$, grossular, $Ca_3Al_2Si_3O_{12}$, almandine, $Fe_3Al_2Si_3O_{12}$ and spessartine, $Mn_3Al_2Si_3O_{12}$. Modelling the position of mineral reactions in P,T space requires an accurate knowledge of the thermodynamic properties of the participating phases including their dependency on pressure, temperature and chemical composition. Considering the wide range of garnet compositions, it is almost impossible to measure these properties for all relevant compositions for geologic P,T conditions. Therefore, in the past years increasing effort has been put into the illumination of the physical concepts that link the thermodynamic properties of a phase with its structure. Along these lines, the present study shows how potential energy calculations and Monte Carlo simulations can provide valuable insight into the mixing behaviour of solid solutions.

The aluminosilicate garnets offer a good model system for the purpose of developing such basic concepts. The end-member phases and the constituent binaries have received intensive phase equilibrium, thermodynamic and crystal-chemical study (see, e.g. Geiger 1999 for a review). For nearly all of the binaries, deviations from ideal, i.e. linear mixing, have been reported for either of the thermodynamic mixing properties such as volume, V^{mix}, enthalpy, H^{mix}, free energy, G^{mix} and vibrational entropy, $S^{mix,vib}$ (Newton et al. 1977; Haselton and Westrum 1980; Geiger et al. 1987; Berman 1990; Berman and Koziol 1991; Ganguly et al. 1993; Gavrieli et al. 1996; Geiger and Feenstra 1997). Besides, it appears that the magnitude of the non-ideal mixing is correlated with the size difference between the substituting cations on the X site (Geiger and Rossman 1994). Indeed, the largest deviations from ideal mixing are observed in the pyrope ($Mg_3Al_2Si_3O_{12}$)-grossular ($Ca_3Al_2Si_3O_{12}$) binary which, therefore, makes it an excellent model system for the study of non-ideal thermodynamic mixing behaviour.

Since Menzer (1928) solved the garnet structure, a number of X-ray structure refinements on natural and synthetic garnets have revealed its response to variable chemical compositions, as well as to changes in extensive parameters like pressure and temperature (e.g. Novak and Gibbs 1971; Meagher 1975; Geiger and Armbruster 1997; Bosenick and Geiger 1997; Hazen and Finger 1978; Ungaretti et al. 1995; Merli et al. 1995; Zhang et al. 1998). It should be stressed that these studies deal only with long-range structural properties which give an averaged picture of the structure and do not account for local structural heterogeneities. The thermodynamic mixing properties will, however, critically depend on the mechanism by which the garnet lattice accommodates different-sized X site cations in a solid solution. The corresponding local structural properties have come under investigation only relatively recently using spectroscopic methods such as XANES (Quartieri et al. 1995), XAFS (Quartieri et al. 1999) and HMIR (Boffa Ballaran et al. 1999). Since simulation studies are able to provide highly detailed information at the level of individual atoms and their interactions, the present study uses static lattice energy calculations to study the local structural response to Ca/Mg cation exchange in garnet.

Furthermore, cation-ordering processes in solid solutions may have a profound influence on phase-equilibrium boundaries. Although variations in enthalpy associated with cation ordering are relatively small, already small changes in the degree of order can result in a considerable lowering of the configurational entropy. Apart from situations where a phase exhibits long-range order, it is not only experimentally difficult to determine its cation distribution but also to derive the corresponding configurational entropy. Computational studies have proven to be a powerful tool for the study of Al/Si ordering processes in phases such as sillimanite (Bertram et al. 1990), leucite (Dove et al. 1993) and gehlenite and cordierite (Thayaparam et al. 1994 and 1996). In these studies, static lattice energy calculations were used to investigate the ordering interaction energies and their different contributions to ordering phase transitions. Monte Carlo methods have been used to determine the ordering temperatures (Thayaparam et al. 1996; Dove et al. 1996). A further combination with statistical-mechanical methods has led directly to expressions for thermodynamic quantities such as configurational entropies (Meyers et al. 1998; Dove 1999).

Aluminosilicate garnets are cubic. Their space group ($Ia\bar{3}d$) does not allow the occurrence of long-range cation order, because there is only one single independent crystallographic dodecahedral, octahedral and tetrahedral site. Any long-range order, therefore, that may occur would result in a space group lowering. While aluminosilicate garnets are treated as having complete random X site cation disorder, evidence for partial cation ordering has been reported for the pyrope-grossular solid solution. Based on the observation of forbidden reflections in a single-crystal X-ray study on a synthetic garnet of composition $Py_{90}Gr_{10}$, Dempsey (1980) proposed a space group lower than $Ia\bar{3}d$ caused by cation ordering. However, apart from a lowering of space group symmetry, multiple diffraction is as likely a source for the forbidden reflections (Rossmanith and Armbruster 1995; Nuber and Schmetzer 1982). Based on the observation of small compositional ranges with negative molar volumes of mixing (ΔV^{mix}) in almandine-grossular and pyrope-grossular solid solutions, Newton and Wood (1980) introduced the model of equivalent site substitution. According to this crystal-chemical model, a certain degree of cation ordering should exist for compositions near the smaller cation end-member component (i.e. almandine and pyrope). This is because the substitution of the larger Ca atom into the structure of the smaller cation end-member is thought to produce large localized site deformations and thus "forbidden regions" which prohibit the incorporation of additional "large" cations in the vicinity. However, more recent investigations do not support the existence of negative volumes of mixing in any of the aluminosilicate garnet binaries. Direct experimental evidence that the divalent

X site cations do not mix completely randomly, but that short-range order of Ca and Mg exists in garnets, was first given by ^{29}Si MAS NMR spectroscopic measurements on synthetic pyrope-grossular solid solutions (Bosenick et al. 1995). Moreover, an extension of this study showed that small differences in the degree of short-range order can be quenched in from high temperature and high pressure (Bosenick et al. 1999).

The analysis of the ^{29}Si NMR spectra of pyrope-grossular garnets is, however, not unequivocal. As discussed by Bosenick et al. (1995), ^{29}Si NMR spectroscopy records both the X site cation distribution in the first and second dodecahedral coordination shells around the ^{29}Si nuclei. This leads to a total of 15 chemically different local dodecahedral environments, each of which can correspond to an individual NMR resonance. Not all of these 15 possible resonances are experimentally observable. This is partly because for the individual compositions some of the environments have a very low occupancy and partly because some of the chemical shifts of certain environments are very similar. The first aspect results in non-measurable resonance intensities while the second results in peak overlapping. Taken together, the measured resonance intensities cannot be completely assigned to specific X site environments which, therefore, prevents a fully quantitative determination of the relative site occupancies. As a consequence, the driving forces behind the short-range ordering cannot be established in detail. This, however, is necessary for a reliable estimation of configurational entropies (Putnis and Vinograd 1999).

Accordingly, the question of Ca/Mg ordering in pyrope-grossular solid solutions may have reached the current limits of experimental methodology. Likewise, we have the more general questions of dodecahedral ordering in aluminosilicate garnets and its possible effect on thermodynamic properties. Of course, additional spectroscopic measurements could provide not only more but eventually more accurate data. However, it is uncertain whether they can lead to a reasonable model for the observed short-range cation order behaviour in garnet.

With reference to the above-mentioned simulation studies, which analyzed the factors determining Al/Si ordering in diverse minerals, we had hoped to unravel the ordering behaviour of the pyrope-grossular solid solution applying similar computational methods. As will be shown, our attempt was partially successful. To begin with, we analyze the goodness of the empirical potential model for the simulation of aluminosilicate garnets in general. Then, we will analyze the mechanism by which the garnet structure responds to the exchange of different-sized X site cations. Subsequently, ordering interaction energies are determined for nearest, next-nearest and more distant neighbours of Mg-Mg and Ca-Ca pairs. This has been done over a range of compositions across the join and it will be shown that the interaction energies are independent of composition. In the second part of this study, we use the derived interaction energies for Monte Carlo simulations. In particular, we make use of the method of thermodynamic integration to determine the effect of short-range order on thermodynamic properties such as the configurational entropy. Finally, the effect of ordering on thermodynamic properties will be discussed and an outlook for linking NMR spectra with empirical models will be given. We start, however, in the following section with a summary of some crystal-chemical aspects of aluminosilicate garnets.

The crystal structure of garnets

The response of the diffraction-averaged properties of the garnet structure to changes in pressure, temperature and chemical composition has been well documented (Zemann 1962; Born and Zemann 1964; Novak and Gibbs 1971; Hazen and Finger 1978; Meagher 1980; Armbruster et al. 1992; Merli et al. 1995; Geiger and Feenstra 1997; Zhang et al. 1998). In the following we summarize some features of the garnet structure which were used for our analysis. As mentioned above, aluminosilicate garnets are cubic and crystallize in space group $Ia\bar{3}d$ (Menzer 1928). Their structure is composed of a three-dimensional network of alternating, corner-sharing SiO_4 tetrahedra and AlO_6 octahedra. The resulting large cavities, that have the shape of triangular dodecahedra, accommodate the divalent cations (Fig. 1). The garnet structure is characterized by extensive edge-sharing between the coordination polyhedra: each tetrahedron shares two opposite edges with dodecahedra, each octahedron shares six edges with neighbouring dodecahedra and, in addition, each dodecahedron shares four edges with other dodecahedra. Only 2 of the 18 dodecahedral edges are unshared. The XO_8 dodecahedra are interconnected such that they build a three-dimensional network. As a consequence,

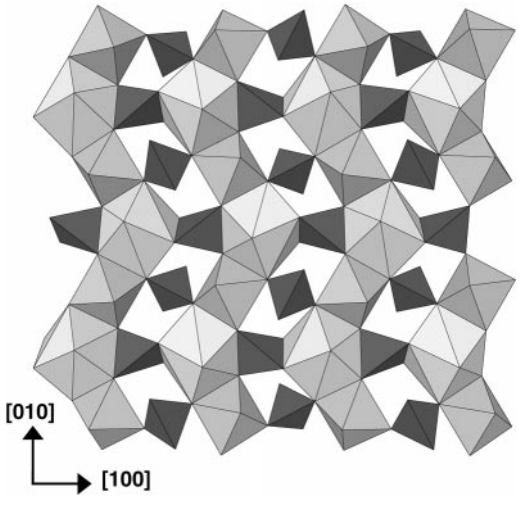

Fig. 1 Polyhedral model of the garnet structure showing the three different coordination polyhedra and their linkages

any substitution on the X site affects the geometry of all other polyhedra.

All polyhedra of the garnet structure are distorted from an ideal geometry. In the long-range averaged structure, the distortions of the polyhedra appear to change continuously as a function of composition. These structural changes can alternatively be described in terms of varying unit-cell dimension or changes in the average radius of the X site cations. The SiO_4 tetrahedra are elongated along their $\bar{4}$ axis, and they become less distorted with increasing size of the X site cation, i.e. in pyrope-grossular solid solutions with increasing Ca content. The AlO_6 octahedra are distorted along the [1 1 1] direction. In garnets with small to medium-sized X site cations, the octahedra are elongated along the $\bar{3}$ axis and the unshared O-O edges are significantly longer than the shared O-O edges. For garnets having a unit-cell dimension greater than about 11.70 Å or, alternatively, an X site radius above ≅ 1.0 Å, the octahedron is flattened along the [1 1 1] direction and the shared edges become longer than the unshared edges (Novak and Gibbs 1971).

Although garnets are classified as orthosilicates, their structure has been described as framework-like (Zemann 1962; Geiger and Feenstra 1997). The changes in the framework resulting from substitution of different-sized divalent cations on the X site is then interpreted by rigid tetrahedral rotation (Born and Zemann 1964; Geiger and Feenstra 1997). The description rigid is, however, slightly misleading. Unlike many true framework silicates, the garnet framework is so tightly constrained, that it does not allow for rigid unit modes (RUMS) (Hammonds et al. 1998). Therefore, tetrahedral rotation results in a simultaneous distortion of the tetrahedra and octahedra that are building the framework. The garnet structure can also be described as containing two types of polyhedral chains which lie parallel to the three crystallographic axes: (1) a chain of edge-sharing tetrahedra and dodecahedra and (2) a chain of corner-sharing tetrahedra and octahedra (Fig. 1).

Interatomic potential model

Basic empirical potentials

The present lattice energy calculations have been performed with the program GULP (General Utility Lattice Program) written by Julian Gale (Gale 1997). The background behind the lattice energy minimization technique has been well documented (e.g. Price et al. 1987; Catlow 1988; Dove 1989; Winkler et al. 1991). The pair interaction between two atoms is modelled as a sum of long-range Coulomb interactions, short-range repulsive interactions, and for polarizable ions dispersive interactions of the form:

$$\varphi(r) = \frac{Q_1 Q_2}{4\pi\varepsilon_0 r} + B \cdot exp\left(-\frac{r}{\rho}\right) - \frac{A}{r^6} \quad . \tag{1}$$

The first term in the potential function is the Coulomb energy: Q_1 and Q_2 are the charges on the ions, ε_0 is the permittivity of free space and r is the interionic distance. The second term is the Born-Mayer repulsive energy which, together with the dispersive last term in Eq. (1) is known as the Buckingham interaction. The parameters B, ρ and A are empirical constants which depend on the atom pair. The cations are represented as rigid ions and formal charges are assumed for their Coulomb interactions. To account for the polarizability of oxygen, it is treated using a shell model, i.e. a combination of a massless charged shell and a central core that has all the ionic mass and the residual ionic charge. The core and the shell interact through a harmonic interaction of the form:

$$\varphi(d) = \tfrac{1}{2} K d^2 \quad , \tag{2}$$

where d is the separation between the centres of core and shell and K is the force constant of the interaction. Covalent bonding is accounted for by the use of bond-bending potentials:

$$\varphi(\theta) = \tfrac{1}{2} k(\theta - \theta_0)^2 \quad , \tag{3}$$

where θ is the O-Si-O or O-Al-O bond angle and θ_0 is the respective angle of the undistorted polyhedron, i.e. $\theta = 109.47°$ for SiO_4 tetrahedra and $\theta = 90°$ for AlO_6 octahedra. The complete set of parameters used in the calculations is given in Table 1. The lattice energy calculations do not include the effects of lattice vibrations and therefore correspond technically to classical simulations of crystals at $T = 0$ K.

Search for the best Ca···O potential

The be-all and end-all of simulation studies is to have a reliable model. As it is generally possible and frequently necessary to adjust the basic model to the system of interest, one has to ensure that the properties being investigated are not built into the model from the start. To overcome this problem, transferable models have been developed which use empirical potential parameters that have been fitted to a wide range of mineral structures (Catlow 1988; Price and Parker 1988; Dove 1989). Nevertheless, before applying the model with confidence to the system of interest, its predictive power should be tested. Of course, depending on which questions will be addressed, the conception about the goodness of the model may vary. Accordingly, the issues being addressed to prove the reliability of the model can vary as well.

Any reliable model should simulate, as well as possible, the physical and structural properties of the material under investigation. In addition, for our purposes, a successful model should be able to reproduce the compositionally dependent structural properties of garnet, such as described above. As a start, we therefore analyzed a variety of calculated garnet structures and compared them with experimental data. We modelled aluminosilicate end-member garnets with different

Table 1 Empirical potential parameters used in this study as defined by Eqs. (1)–(3)

	Buckingham potential between cation cores and O shells			Reference[a]
	B (eV)	ρ (Å)	A (eV/Å^6)	
Si^{4+} ···· O^{2-}	1283.9073	0.3205	10.662	1
Al^{3+} ···· O^{2-}	1460.3	0.2991		2
O^{2-} ···· O^{2-}	22764.0	0.1490	27.880	1
X^{2+} ····O^{2-}				
Mg-1	1428.50	0.29		3
Mg-2	1275.20	0.30		6
Mg-3	2457.20	0.26		5
Ca-1	6958.30	0.25		4
Ca-2	15944.10	0.24		Modified after (4)
Ca-3	2272.70	0.30		5
Ni	683.50	0.33		7
Co	696.30	0.34		7
Zn	499.60	0.36		7
Fe	694.10	0.34		7
Mn	715.80	0.35		7
Cd	868.30	0.35		7
Sr	17313.50	0.24		4
Ba	29573.60	0.24		4
Core-shell interaction between O core and O shell	K (eV/Å^{-2})			
$O_{Core}^{+0.8482} \cdots O_{Shell}^{-2.8482}$	74.9200			1
Bond-bending interactions	k (eV/rad^2)	θ_0 (°)		
O^{2-}-Si^{4+}-O^{2-}	2.09724	109.47		1
O^{2-}-Al^{3+}-O^{2-}	2.09724	90.9		1

[a] 1, Saunders et al. (1984); 2, Catlow et al. (1982); 3, Price and Parker (1988); 4, Post and Burnham (1986); 5, Bush et al. (1994); 6, Sangster and Stoneham (1981); 7, Lewis (1984)

divalent X site cations on the dodecahedra (e.g. Fe, Mn, Co, Ni, Zn), notwithstanding if the respective cation can in reality be accommodated in aluminosilicate garnets (e.g. Ba, Sr). Several published cation-oxygen (X···O) pair interactions – in the following loosely referred to as X potentials – were used, including, in particular, three different potentials for Mg···O and Ca···O interactions (Table 1).

A major change in the aluminosilicate garnet structure with increasing unit-cell dimension is that the shared O-O edges of the AlO_6 octahedra become longer than the unshared O-O edges. Figure 2 shows the variation of the two O-O bond lengths as a function of unit-cell dimension. The data marked with an asterisk were calculted with the Mg-1 and Ca-1 potentials, which were previously used in simulation studies of silicate minerals (Price et al. 1987; Dove 1989; Winkler et al. 1991). We plotted also the mean O-O bond lengths derived from X-ray diffraction studies undertaken at room temperature, 100 and 500 K on synthetic aluminosilicate garnets of end-member and solid-solution compositions (Armbruster et al. 1992; Geiger et al. 1992; Armbruster and Geiger 1993; Ganguly et al. 1993). The calculated O-O bond lengths vary nearly linearly with increasing unit-cell dimension. This trend is in good agreement with the experiments. The only data that do not follow this linear

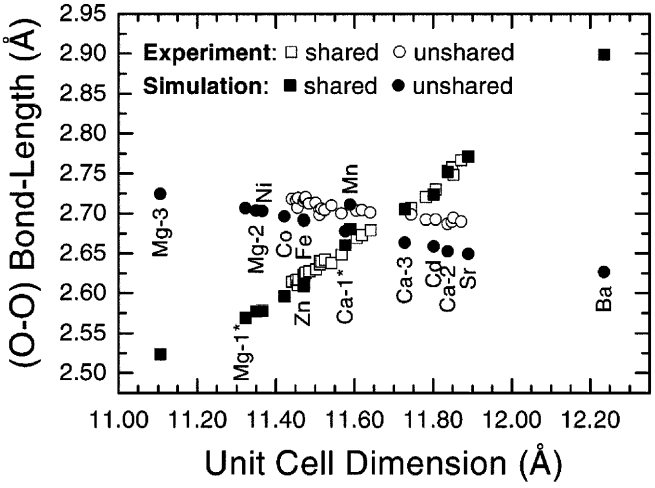

Fig. 2 Variation of the shared and unshared octahedral O-O edges in garnet as a function of the unit-cell length calculated using different X···O potentials. The labeling of the data corresponds to the labeling of the potentials as given in Table 1. For comparison, experimental data of various aluminosilcate garnets (Geiger et al. 1991; Ganguly et al. 1992; Armbruster and Geiger 1993; Armbruster et al. 1992) are plotted which indicate a nearly linear change in the octahedral O-O edges with increasing unit-cell dimension

trend are those calculated using an Mn^{2+} potential. However, simulations with cations like Sr and Ba follow the linear trend, although such garnet compositions have not been found in nature or synthesized in the laboratory. Hence, the potential model calculations are capable of predicting the overall response of the garnet structure to the incorporation of different-sized divalent cations onto the dodecahedral sites.

A detailed comparison of experimentally determined structural properties of pyrope (Armbruster et al. 1992) and grossular (Ganguly et al. 1993) with those obtained from simulations using three different potentials for Mg

Table 2 Comparison between observed and calculated structural parameters for the garnet end-members pyrope and grossular. The structural parameters of the observed structures were calculated using fractional coordinates and unit-cell constants determined by Armbruster et al. (1992) for pyrope and Ganguly et al. (1993) for grossular. The different potentials are from the following sources: Mg-1 (Price and Parker 1988); Mg-2 (Sangster and Stoneham 1981); Mg-3 and Ca-3 (Bush et al. 1994); Ca-1 (Post and Burnham 1986); Ca-2 (modified; see text)

		Pyrope				Grossular			
		Observed	Calculated			Observed	Calculated		
		293 K	Mg-1	Mg-2	Mg-3	293 K	Ca-1	Ca-2	Ca-3
Unit-cell dimension and fractional coordinates of the oxygen atoms									
a_0 (Å)		11.4520	11.3226	11.3504	11.1063	11.8480	11.5774	11.8378	11.7278
x		0.0329	0.0322	0.0324	0.0316	0.0382	0.0364	0.0401	0.0372
y		0.0503	0.0525	0.0519	0.0572	0.0453	0.0495	0.0460	0.0459
z		0.6533	0.6528	0.6527	0.6539	0.6514	0.6510	0.6495	0.6507
Tetrahedron									
Si-O(1)	4x[a]	1.634	1.633	1.634	1.618	1.646	1.641	1.650	1.645
O(1)-O(2)	2x	2.497	2.501	2.502	2.483	2.572	2.563	2.617	2.566
O(1)-O(3)	4x	2.751	2.747	2.748	2.719	2.745	2.737	2.733	2.744
⟨O-O⟩		2.666	2.665	2.666	2.640	2.687	2.679	2.694	2.685
O(1)-Si-O(2)	2x	99.62	99.91	99.93	100.23	102.71	102.65	104.93	102.53
O(1)-Si-O(3)	4x	114.61	114.45	114.44	114.28	112.95	112.99	111.79	113.05
Angular distortion (%)[b]		9.52	9.23	9.21	8.92	6.48	6.55	4.33	6.66
Edge-length distortion (%)[b]		4.23	4.10	4.09	3.96	2.86	2.89	1.90	2.94
Angle variance σ^{2c}		59.98	56.38	56.17	52.70	27.96	28.52	12.52	29.48
Tetrahedral angle of rotation α[d]		27.5	28.4	28.08	30.75	24.66	26.56	24.57	24.78
Octahedron									
Al-O(1)	6x	1.886	1.866	1.868	1.857	1.926	1.887	1.911	1.898
O(1)-O(4) (shared)	6x	2.616	2.569	2.577	2.524	2.758	2.660	2.752	2.705
O(1)-O(5) (unshared)	6x	2.717	2.707	2.704	2.725	2.689	2.678	2.652	2.663
⟨O-O⟩		2.667	2.638	2.640	2.624	2.724	2.669	2.702	2.684
O(1)-Al-O(4)	6x	87.85	87.01	87.26	85.62	91.44	89.62	92.11	90.90
O(1)-Al-O(5)	6x	92.15	92.99	92.74	94.38	88.56	90.38	87.89	89.10
Angle variance[c]		5.04	9.77	8.21	20.97	2.26	0.16	4.88	0.88
Angular distortion (%)[b]		2.39	3.33	3.05	4.87	1.60	0.42	2.35	1.00
Edge-length distortion (%)[c]		5.00	6.89	6.32	10.04	3.42	0.88	4.99	2.10
(O-O)sh – (O-O)ush		−0.10	−0.14	−0.13	−0.20	0.07	−0.02	0.10	0.04
Dodecahedron									
X1-O(4)	4x	2.197	2.175	2.181	2.137	2.322	2.266	2.352	2.295
X2-O(4)	4x	2.340	2.287	2.300	2.194	2.487	2.378	2.478	2.452
⟨X-O⟩		2.269	2.231	2.241	2.165	2.405	2.322	2.415	2.374
O(1)-O(2)	2x	2.497	2.501	2.502	2.483	2.572	2.563	2.617	2.566
O(1)-O(4)	4x	2.616	2.569	2.577	2.524	2.758	2.660	2.752	2.705
O(4)-O(6)	4x	2.707	2.643	2.662	2.508	2.971	2.823	3.007	2.929
O(4)-O(7)	2x	2.777	2.721	2.734	2.613	2.859	2.754	2.805	2.833
O(1)-O(7)	4x	3.307	3.271	3.280	3.199	3.452	3.370	3.470	3.419
O(7)-O(8)	2x	3.822	3.731	3.753	3.583	4.118	3.925	4.127	4.048
⟨O-O⟩		2.929	2.880	2.892	2.793	3.101	2.994	3.112	3.062
O(1)-X(2)-O(2)	2x	69.24	70.18	70.01	71.06	67.24	68.88	67.62	67.99
O(1)-X(2)-O(4)	4x	70.35	70.25	70.15	71.28	69.88	69.85	69.41	69.38
O(4)-X(2)-O(6)	4x	73.19	72.57	72.83	70.77	76.22	74.84	76.95	76.10
O(4)-X(2)-O(7)	2x	72.81	72.99	72.92	73.11	70.16	70.74	68.93	70.57
O(1)-X(2)-O(7)	4x	93.51	94.24	94.07	95.23	91.66	93.03	91.81	92.10
O(7)-X(2)-O(8)	2x	109.50	109.30	109.35	109.47	111.78	111.22	112.75	111.28
(X2–0) – (X1-O)		0.14	0.11	0.12	0.06	0.16	0.11	0.13	0.16

[a] Multiplicity
[b] Renner and Lehmann (1986)
[c] Robinson et al. (1971)
[d] Born and Zemann (1964)

and Ca is presented in Table 2. In addition to a simple comparison of bond lengths and angles, it appears that the distortions of the different polyhedra give a clear indication about the appropriateness of the different potentials.

In the case of pyrope, the relation between shared and unshared O-O bond lengths is correctly predicted with all three Mg potentials (Fig. 2). However, on further study of Table 2, the model with the Mg-3 shows various weak points in comparison with the Mg-1 and Mg-2 potentials. For example, with the Mg-3 potential the unit-cell dimension is calculated as 11.1063 Å, which is too low. In addition, the octahedra are distorted more than twice as much as they should be. This is apparent from the angle variance, which is 20.97 using the Mg-3 potential. In comparison, it is 9.77 and 8.21 when undertaking simulations with Mg-1 and Mg-2. These values are much closer to the experimental value of 5.22. As a final example, we refer to the difference between the two Mg-O bond distances of the dodecahedron, which are also better simulated using the Mg-1 and Mg-2 potentials. The simulations with these two Mg potentials (Mg-1 and Mg-2) give similar results, and it is not straightforward to decide which provides a better model for pyrope. For our further simulations, we decided on Mg-1, because it has already been used in other simulation studies on minerals.

In the case of grossular, the Ca-1 potential, which has frequently been used for simulations of Ca-containing minerals, predicts the lengths of the shared octahedral edges to be shorter than the unshared edges. This is contrary to the actual situation. From a structural point of view, this Ca potential does not simulate grossular, but instead a garnet with a smaller X site cation radius than Ca. From an analysis of Fig. 2 it can be estimated that a garnet structure is modelled with an X site cation which is slightly smaller than Mn^{2+}. Hence, in order to get a better model for grossular, we tried to develop a new Ca potential. We constrained the parameter ρ of the Buckingham potential to be 0.24 Å, because this is equal to the ρ-value in the potentials of Sr and Ba (Post and Burnham 1986), and which is able to simulate an octahedron that is flattened along its $\bar{3}$ axis. The B value of the new potential was obtained by fitting to the structure of CaO. Figure 2 shows that simulations using this modified potential, Ca-2, result in octahedral O-O bond lengths that are in better agreement with experimental findings. However, although this potential is able to model the relation between the shared and unshared O-O bond lengths of the octahedron correctly, it overestimates the flattening of the octahedra. This is apparent in the octahedral angle variance (4.88), angular distortion (2.35) and edge-length distortion (4.99), which are all considerably larger than for the experimentally observed structure (2.26, 1.60 and 3.42, respectively). In addition, our modified Ca-2 potential gives a poor representation of the SiO_4 tetrahedron, because the Si-O bond lengths are slightly too long and the overall distortion too small (see Table 2).

We finally undertook simulations of grossular using a third Ca potential, Ca-3, taken from Bush et al. (1994). This potential gives an octahedron that is correctly flattened along the [1 1 1] direction, but which should be even more distorted. In addition, the resultant unit-cell dimension should be longer. In the case of the Al-O bonds, the Ca-3 potential seems to do less good than the potential Ca-2. The Al-O bonds are calculated to be 1.898 Å with the Ca-3 potential and 1.911 Å with the Ca-2 potential in comparison to an experimental value of 1.926 Å. However, the resulting differences between calculated and observed Al-O bond lengths are for both potentials well below 2%, which is at the level of accuracy from potential model calculations. In the case of the SiO_4 tetrahedron, the Ca-3 potential reproduces the experimentally observed distortions clearly better than Ca-2. Although Ca-3 does not predict the exact degree of distortion for the three different polyhedra, it models the overall structural trends in a correct way and, hence, gives in total the best, albeit least bad, model for grossular. A test of the general transferability of this Ca potential to other minerals is given in the Appendix.

We checked the predictive power of our final model by calculating the energies of IR-active phonons of pyrope and grossular. Figure 3 shows a comparison between the calculated TO phonon modes using Mg-1 and Ca-3 and measured powder IR frequencies (Boffa Ballaran et al. 1999). The observed and calculated energies agree to better than 10% in the case of grossular, whereas in the case of pyrope, the agreement is slightly worse. At energies between 600 and 800 cm^{-1} differences of up to 80 cm^{-1} occur. The mean deviation between observed and calculated energies is about 20 cm^{-1} for both garnets.

Finally, it is worth noting that the empirical potentials being used have been developed in consideration of the derivatives of the energy with respect to the interatomic distances rather than actual energies. The first derivative of energy with respect to interatomic distance determines the structure and the second derivative the elastic constants. It is, therefore, not likely to get the energies correct on an absolute scale. However, differences in energies between different phases and/or different structural states are more likely to be correct, since these differences are closely related to the differentials of the energy. This is important for the present study. Different ordering states are modelled, while the general structural parameters remain unchanged. We are concerned only about the relative energy changes due to different arrangements of Ca and Mg on the dodecahedral sites, and, indeed, as will be discussed later, the energy differences obtained with potential model are in good agreement with electronic structure calculations.

From the above comparison of experimental and simulated structures, it is evident that our model is not perfect. However, it should be kept in mind *that no part of the model has been optimized for garnet*. The level of agreement between model and experiment for structural, as well as physical properties, such as IR frequencies, therefore suggests that the model contains the necessary predictive power to simulate structural and energetic

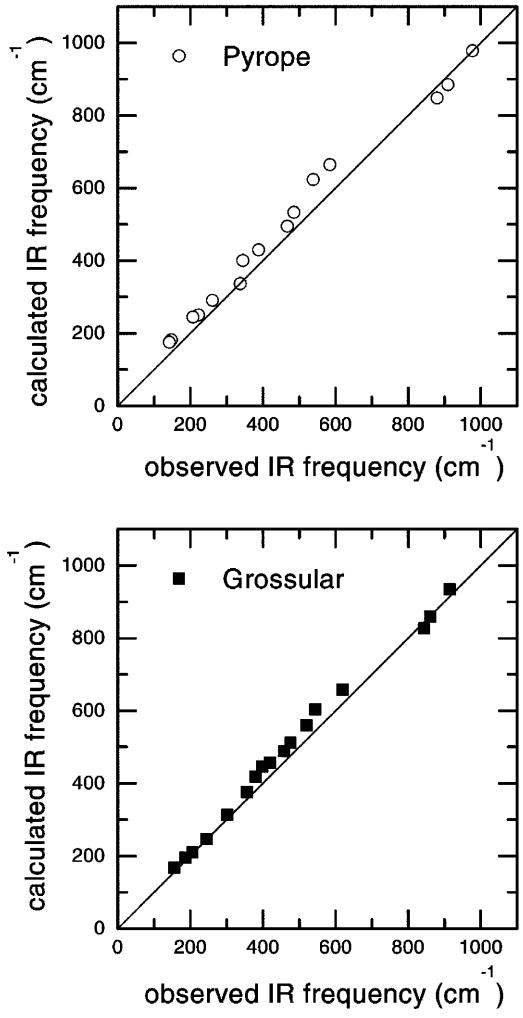

Fig. 3 Comparison between TO modes calculated using the best Ca and Mg potentials (Ca-3 and Mg-1) and observed powder IR frequencies of the end-member garnets pyrope and grossular

properties related to the cation distribution in pyrope-grossular solid solutions with confidence.

Ordering energies

The effect of Ca/Mg ordering in pyrope-grossular solid solutions was investigated by performing calculations in a $1 \times 1 \times 1$ supercell. This *I*-centred unit-cell contains eight formula units and, hence, 64 cations and 96 oxygen atoms. The number of oxygens has to be counted twice because they are modelled using a core-shell model. Therefore, the $1 \times 1 \times 1$ supercell contains 256 species that have to be relaxed. The use of a larger supercell, for example a $2 \times 2 \times 2$ supercell, would contain 2048 species, but is limited partly because of the time and partly because of the extensive computer memory needed for relaxing such large systems. However, a $1 \times 1 \times 1$ supercell contains 24 dodecahedral sites, which is sufficient for the investigation of ordering effects. For comparison, Al/Si ordering in cordierite was studied using 36 tetrahedral sites (Thayaparam et al. 1996), in gehlenite 32 sites (Thayaparam et al. 1994) and in sillimanite 24 sites (Bertram et al. 1990) were used.

The composition of the solid-solution is controlled by the ratio of Ca and Mg cations on the 24 X sites. For several compositions a database of many different random arrangements of Ca and Mg on these 24 dodecahedral sites was built up. For every configuration the coordinates of all the "atoms" (core and shell) and the unit-cell size were relaxed, i.e. the calculations were done at constant pressure. No symmetry constraints were used, but to allow for faster relaxation, the unit-cell was constrained to be of cubic shape. To check the validity of this setup, we also undertook calculations without constraining the shape of the supercell. As will be shown later, the results were very similar.

Calculations in the dilute limit

Local structural response to the substitution of one dodecahedral cation in a garnet end member

Since periodic boundary conditions were used in the calculations, there is only one distinct arrangement for replacing one dodecahedral cation by another in a $1 \times 1 \times 1$ supercell. When replacing one Mg with Ca in pyrope, the unit-cell expands relative to pure pyrope and when replacing one Ca with Mg in grossular, the cell contracts relative to pure grossular (Table 3). When the unit-cell is allowed to relax without any constraints after replacing one divalent cation, it undergoes a more or less tetragonal deformation, where the *c* direction is parallel to the tetrahedra-dodecahedra chain in which the substitution was performed. This is an immediate result of the strong repulsive forces acting between the cations in the dodecahedra-tetrahedra chain (Zemann 1962). A detailed structural picture of how these "foreign" cations (Ca in pyrope and Mg in grossular) are accommodated in their host structures is obtained by analyzing their local environments.

Table 3 Unit-cell dimension and total lattice energy of garnets with one "foreign" X-site cation relaxed in an isotropic supercell and in space group P1

	1 Ca in pyrope	1 Mg in grossular
Isotropic relaxed		
a_0 (Å)	11.3412	11.7136
Utot (eV)	−5397.2091	−5324.1523
Relaxed using no constraints		
a	11.3573	11.6951
b	11.3329	11.7229
c	11.3329	11.7228
Alpha	89.94	89.97
Beta	90.00	90.00
Gamma	90.00	90.00
Utot (eV)	−5397.2118	5324.15755

The substituted foreign cation – like all other atoms in the structure – tries to optimize its local environment. It individually tries to obtain energetically favourable distances and orientations with the surrounding atoms instead of taking on an averaged position. This is evident from Table 4, which summarizes the X-O bond lengths in pyrope-rich and grossular-rich garnets with one foreign X cation each. For example, the Ca-O bond lengths of a single Ca cation in the pyrope-rich garnet are very similar to their values in pure grossular. At the same time, the Mg cations individually try to maintain their distances to the oxygens rather than taking averaged distances. An analogous situation exists in a grossular-rich garnet with one Mg cation. The values of the Mg-O bond lengths are similar to those in pure pyrope and are considerably different from averaged X-O bond distances, which one would obtain from X-ray diffraction methods for this composition.

In addition, all polyhedra in the unit-cell distort relative to their shape in the end-member structures when just one of the 24 X site cations is substituted. As will be discussed below, this is a direct consequence of the non-existence of RUMS in garnets. The bond lengths and internal angles of the SiO_4 tetrahedra and AlO_6 octahedra surrounding the substituted X cation in 1st, 2nd, and 3rd coordination are summarized in Table 5. When

Table 4 Comparison of the calculated X-O bond length (Å) in pyrope-rich and grossular-rich garnet containing one foreign cation

	1 Ca in pyrope			1 Mg in grossular	
	X1-O(4) (Å)	X2-O(4) (Å)		X1-O(4) (Å)	X2-O(4) (Å)
Ca-O	2.295	2.347	Mg-O	2.170	2.417
Mg-O (es)[a]	2.167–2.181	2.284–2.301	Ca-O (es)	2.295–2.303	2.433–2.458
⟨Mg–O⟩[b]	2.176 (8)	2.293 (4)	⟨Ca-O⟩	2.295 (3)	2.448 (4)
Mg-O[c]	2.175	2.287	Ca-O[c]	2.295	2.452

[a] X-O bond length of the dodecahedra edge-shared to the dodecahedron containing the diluting cation
[b] Average over all X-O bond lengths in the unit cell except those of the foreign cation
[c] X-O bond lengths calculated for pure end member

Table 5 Bond length (Å) and angles (°) of the tetrahedra and octahedra surrounding the foreign divalent cation, X, in the 1st, 2nd and 3rd coordination shell for pyrope containing 1 Ca and grossular containing 1 Mg

		1 Ca in pyrope			1 Mg in grossular		
		1st shell	2nd shell	3rd shell	1st shell	2nd shell	3rd shell
Tetrahedra							
X-Si		2.90	3.49	5.31	2.87	3.58	5.47
Si-O		1.632	1.631	1.631	1.646	1.641	1.648
		1.632	1.633	1.635	1.646	1.644	1.641
		1.632	1.634	1.636	1.650	1.646	1.644
		1.632	1.634	1.638	1.650	1.647	1.644
O-O		2.517	2.491	2.496	2.484	2.566	2.570
		2.582	2.501	2.497	2.546	2.570	2.571
		2.720	2.736	2.743	2.772	2.736	2.721
		2.720	2.743	2.745	2.772	2.736	2.745
		2.722	2.754	2.746	2.776	2.748	2.748
		2.722	2.759	2.774	2.776	2.749	2.748
O-Si-O		100.9	99.4	99.5	97.7	102.5	102.8
		104.6	100.0	99.6	101.3	102.9	102.8
		112.8	113.8	113.9	114.5	112.4	111.8
		112.8	114.2	114.4	114.5	112.8	113.0
		113.0	114.9	114.4	114.8	113.3	113.2
		113.0	115.4	115.9	114.8	113.5	113.6
Octahedra							
X-Al		3.20	5.13	6.50	3.25	5.27	6.71
Al-O	From	1.860	1.863	1.861	1.883	1.890	1.892
	To	1.877	1.872	1.872	1.906	1.906	1.900
O(1)-O(4)	From	2.551	2.548	2.562	2.608	2.695	2.698
	To	2.677	2.578	2.576	2.718	2.729	2.706
O(1)-O(5)	From	2.653	2.701	2.702	2.653	2.648	2.661
	To	2.721	2.724	2.710	2.720	2.663	2.665
O(1)-Al-O(4)	From	86.0	86.2	86.8	87.4	88.5	89.1
	To	90.5	87.3	87.2	90.0	89.5	89.3
O(1)-Al-O(5)	From	91.1	92.5	92.8	90.3	90.6	90.7
	To	93.7	93.7	93.0	91.9	91.6	90.9

a large Ca cation is placed in a pyrope-rich host structure, it pushes all neighbouring cations away and thereby deforms the surrounding SiO_4 tetrahedra and AlO_6 octahedra. The largest distortion is in the two tetrahedra that are edge-shared with the dodecahedron in which the substitution takes place (i.e. 1st shell). The Si-O distances in these tetrahedra stay almost constant relative to those in the pyrope end-member (cf. Tables 2 with 4 and 5) but both of the shared O-O edges expand. In pure pyrope they measure 2.502 Å. In the pyrope-rich garnet with one dissolved Ca cation, the O-O edge shared with the Mg dodecahedron lengthens to 2.517 Å and that shared to the Ca dodecahedron on the opposite side to 2.582 Å. The corresponding O-Si-O angles also increase. The angle towards the Ca dodecahedron widens from 99.9° to 104.6°, while that towards the Mg dodecahedron becomes 1.0° larger and measures 100.9°. In addition, to compensate for the incorporation of the larger Ca cation the edge-sharing tetrahedra undergo a slight torsion. This is recognizable through very small changes of the tetrahedral angle of rotation, α, which measures 28.3° at the O-O edge shared to the Mg dodecahedron and 28.1 at the edge shared to the Ca dodecahedron compared to 28.4° in pure pyrope. The four tetrahedra that are corner-shared to the Ca dodecahedron (i.e. 2nd shell) show a greater scatter in the unshared O-O edges lengths than the tetrahedra of the third coordination shell. The latter still show some variation in the Si-O bond distances. The AlO_6 octahedra surrounding the Ca dodecahedron are also deformed relative to their shape in pyrope. As in the case of the tetrahedra, the octahedra are most affected through an expansion of the O-O edges shared to the Ca dodecahedron. These O-O edges measure 2.677 Å, which is closer to the length in grossular (2.705 Å) than to their length in pyrope (2.569 Å). The Al-O distances, the two different O-O edge lengths and the two different O-Al-O angles are also affected. The variation in these lengths and bond angles becomes smaller with increasing distance from the substituted foreign cation. For example, the O(1)-Al-O(4) angles of the octahedra edge-shared with the Ca dodecahedron (1st shell) vary between 86.0° and 90.5°, while those of the octahedra in the 2nd coordination shell vary between 86.2° and 87.3° and those of the 3rd shell have nearly similar values between 86.8° and 87.2°.

On the other hand, when 1 Mg is substituted in a grossular supercell it draws the surrounding cations nearer. By this means, the shape of the neighbouring tetrahedra and octahedra becomes more similar to those in pyrope. In analogy to the substitution of 1 Ca in a pyrope-rich host structure, it is observed that the Si-O bond lengths remain almost constant but the O-O edges show distinct changes. Here, however, both of the shared O-O edges shorten. The O-O edge shared with the Mg dodecahedron shortens more than that shared to the Ca dodecahedron. The O-Si-O angles also change in an opposite manner. In grossular the smaller of the two O-Si-O angles measures 102.5°. With the substitution of Mg it decreases to 97.7° towards the Mg dodecahedron, but on the side of the Ca dodecahedron it decreases less by about 1° to 101.3°. The O-O edges shared between the Mg dodecahedron and the six surrounding octahedra decrease to 2.608 Å compared to a value of 2.705 Å in grossular. More analogies between the local structural changes around a substituted Ca atom in an Mg-rich host structure and a substituted Mg in a Ca-rich host structure can be extracted from Table 5.

To summarize, the substitution of Mg or Ca as "foreign" cations produces strong local distortions in the host structure effecting all polyhedra in the unit-cell. This leads, in particular, to a range of cation-oxygen bond lengths, which in turn leads, for example, to measurable line broadening of the absorbance bands in infrared spectra (Boffa Ballaran et al. 1999). The strain field induced by a foreign X cation can be estimated to have a minimum radius of 5.5 Å, because distortions from the end-member geometry are visible throughout the whole $1 \times 1 \times 1$ supercell. The calculated changes in the tetrahedra and octahedra can be interpreted such that Ca cations preserve grossular-like and Mg cations pyrope-like local environments.

Relative arrangement of two foreign X cations and their interaction

If one substitutes two Ca cations in a pyrope-like structure (or two Mg in a grossular-like structure), one has seven different ways to arrange the two foreign cations in a $1 \times 1 \times 1$ supercell. Each of these arrangements corresponds to a distinct distance between two X sites. Figure 4 shows a section of a polyhedral model of

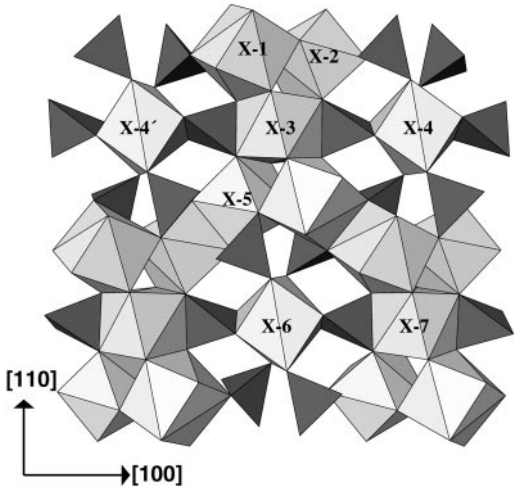

Fig. 4 Portion of the garnet structure showing the dodecahedral framework and its linkage to the SiO_4 tetrahedra. The AlO_6 ocatahedra are, for clarity, not shown. Within one unit-cell, the configuration of two dodecahedral sites is defined by one of seven arrangements which correspond to different distances (d): d1 between (*X-1*) and (*X-2*); d2 between (*X-2*) and (*X-4*); d3 between (*X-3*) and (*X-4*); d4 between (*X-1*) and (*X-5*); d5 between (*X-2*) and (*X-5*); d6 between (*X-3*) and (*X-6*) and d7 between (*X-3*) and (*X-7*). See Table 5 for approximate distances between the sites and the total number of the different neighbours

the garnet structure that illustrates the different possible cation arrangements. The closest arrangement of two Ca cations in a pyrope host structure results, when they are placed in two dodecahedra that are edge-shared to each other. We define this arrangement as distance 1 or d1. The second-nearest arrangement of two foreign X cations (distance 2 or d2) results from placing them in two dodecahedra that are shared to the same tetrahedron, where one is edge-shared and the other corner-shared. Two dodecahedra that are edge-shared to the same tetrahedron are described as distance 3 neighbours (d3). Distance 4 (d4) and distance 5 (d5) neighbours are edge-shared to the same dodecahedron, whereby the first are, in addition, corner-shared to the same tetrahedron. Dodecahedra of distance 6 (d6) and distance 7 (d7) neighbours share no common polyhedron or edge but belong to neighbouring dodecahedra-tetrahedra chains.

For these seven different possible arrangements, lattice energy calculations have been undertaken for 2 Ca cations in a pyrope host and for 2 Mg cations in a grossular host. The calculations were made both by constraining the unit-cell to be of cubic shape and by allowing a unit-cell of $P1$ symmetry. The relative total lattice energies of the different arrangements are compared in Fig. 5 as a function of the interatomic distance between the two foreign cations. The relative total lattice energy is given as the difference between the total lattice energy of the respective arrangement and that of the lowest energy arrangement (i.e. configuration d1) divided by the multiplicity, z, of the arrangement according to periodic boundary conditions. For example, only two tetrahedra and two dodecahedra of a tetrahedra dodecahedra chain fit into one unit-cell. For a certain dodecahedron (e.g. X-3 in Fig. 4), the distance 3 neighbour in one direction (X-4 in [1 0 0] direction) is, because of periodic boundary conditions, in a $1 \times 1 \times 1$ supercell identical to the dodecahedron in opposite direction (X-4′). Hence, the distance 3 configuration has a multiplicity $z = 2$. The multiplicity of distance 4 neighbours is also 2, that of distance 5 and 6 neighbours is 4 and that of distance 7 neighbours is 8. The multiplicity of the other arrangements is unity.

It can be seen from Fig. 5 that there is no direct correlation between the relative lattice energies and the interatomic distance between the two foreign cations. Moreover, the relative total energy of four of the seven arrangements (d1, d2, d6 and d7) is almost the same, indicating that these arrangements are equally likely to occur. The most surprising result is, however, that the nearest-neighbour interaction is of no particular significance. Unlike, for example, our experience with Al/Si ordering, where the Al-Al repulsion is strongest for nearest neighbours, both dodecahedral cations, Ca as well as Mg, like to be placed directly next to a cation of the same kind. Exactly the opposite behaviour is predicted for the placement of large Ca cations in pyrope-rich garnets according to the equivalent site model (Newton and Wood 1980). From our simulations, the energetically most unfavourable configuration is d3, which is only via the third shortest distance. Here, the two substituted foreign cations occupy dodecahedra that are edge-shared to the same SiO_4 tetrahedron. The configurations d4 and d5 are also associated with higher energies, but these additional terms are only about half that of arrangement d3. Interestingly, the relative lattice energies for the different configurations are approximately the same whether two Ca atoms are placed in a pyrope-rich structure or two Mg cations occur in a grossular-rich structure. The calculations using $P1$ symmetry and those constraining the unit-cell to maintain its cubic shape give very similar results (Table 6). Since the latter are much faster (by a factor of 20 and more), we used isotropic constraints in calculations of arrangements in less dilute systems.

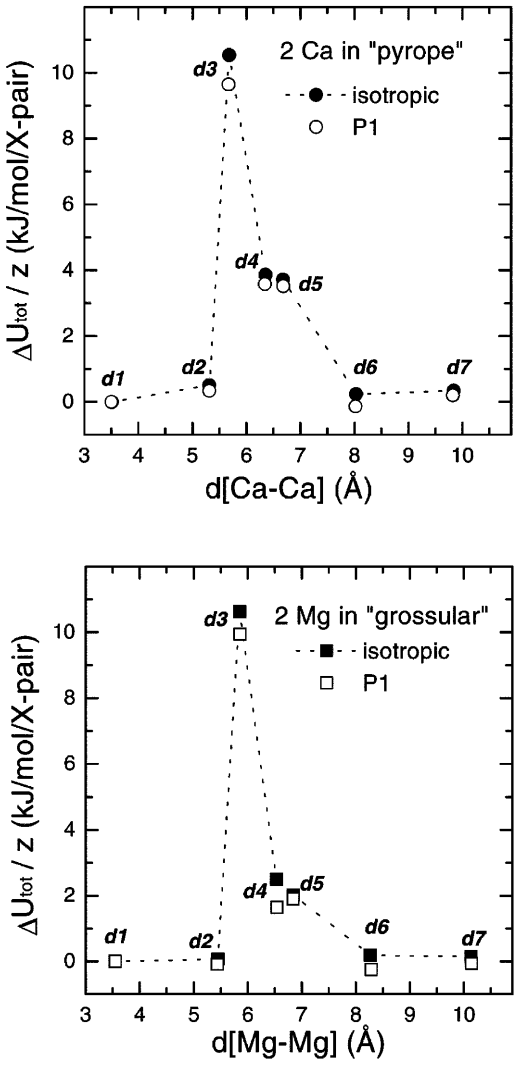

Fig. 5 Relative total lattice energy of the different arrangements (top) for two foreign Ca cations in pyrope-rich structure and (bottom) for 2 Mg substituted in a grossular-rich structure. The energies are plotted as a function of the interatomic distance between the two foreign X-site cations

Table 6 The relative atomic interaction constants J_i (kJ mol^{-1} per X-pair). The Js have been normalized so that J_1 equals zero for all compositions

	d(X-X)[b] (Å)	N[c]	No. of Ca							
			2[a]	**3**	**4**	**6**	**12**	20	21	22
			No. of Mg							
			22	21	20	18	12	**4**	**3**	**2**
$\mathbf{J}_1$	3.511	4	0.00	0.00	0.00	0.00	0.00	0.00	0.00	0.00
$\mathbf{J}_2$	5.314	8	0.06	0.12	0.05	−0.14	0.26	0.02	0.05	0.01
$\mathbf{J}_3$	5.680	2	1.32	1.28	1.23	1.31	1.50	1.34	1.28	1.33
$\mathbf{J}_4$	6.356	8	0.48	0.31	0.29	0.17	0.43	0.27	0.17	0.31
$\mathbf{J}_5$	6.679	4	0.46	0.39	−0.01	0.33	0.39	−0.06	0.24	0.25
$\mathbf{J}_6$	8.032	4	0.03	−0.02	−0.03	0.01	0.24	0.11	−0.04	0.02
$\mathbf{J}_7$	9.837	8	0.04	0.03	0.11	0.01	0.30	0.08	−0.02	0.02
Configurations[d]			7	26	20	50	60	20	26	7
R value[e]			1	0.786	0.976	0.972	0.985	0.969	0.735	1

[a] The interaction constants were determined for the more dilute cations in the supercell, i.e. those which are in boldface
[b] Distance between corresponding dodecahedral sites in the case of pyrope
[c] Number of type J_i neighbours
[d] Number of configurations that have been calculated and relaxed. In the case of two and three foreign atoms all possible configurations were calculated. For the less dilute compositions, the given number of arbitrary configurations were calculated
[e] R value for multilinear regression of J values to Eq. (4)

Calculations in long supercells

To ensure that the finding that configuration d3 is energetically the most unfavourable configuration, is not an artefact resulting from the use of an insufficiently large supercell, additional calculations were performed in long supercells. As discussed above, only two dodecahedra of a dodecahedra-tetrahedra chain fit into one unit-cell. In a $2 \times 1 \times 1$ supercell the chain contains four dodecahedral sites along [1 0 0]. Placing two foreign cations in neighbouring dodecahedra in such a tetrahedra-dodecahedra chain corresponds to a single d3 arrangement. This arrangement is equivalent to a d3 arrangement in a perpendicular chain, albeit having the multiplicity 2. Hence, the relative lattice energies of the two arrangements, accounting for their multiplicity, should be the same. The relative total lattice energy for two Ca cations in a pyrope-rich supercell is 9.2 kJ mol^{-1} per Ca-pair for the d3 arrangement in [1 0 0] direction and 11.0 kJ mol^{-1} per Ca-pair perpendicular to it. Although these two values differ by ~18%, they are clearly larger than the relative lattice energies of any of the other configuration (Fig. 5). Hence, the arrangement d3 is, indeed, energetically the least favourable of the seven possible relative arrangements for a system with two foreign X cations.

The calculations were further extended to a $3 \times 1 \times 1$ supercell. Here, the tetrahedra dodecahedra chain in [100] direction contains six dodecahedral sites. Total lattice energies were determined as a function of the interatomic distance between the two foreign X cations in this chain. Calculations were undertaken for the following three distinguishable arrangements: (1) placing two foreign cations in the first two, i.e. neighbouring dodecahedra, (2) placing them in the first and the third dodecahedra and (3) placing them in the first and the fourth dodecahedra. Figure 6 shows the relative lattice energies of these arrangements for 2 Ca in a pyrope host and for 2 Mg in a grossular host structure. The total lattice energies of the different arrangements decrease linearly as a function of the reciprocal cubed interatomic distance ($1/r^3$). This implies that the differences in the lattice energies for the different cation configurations result primarily from strain effects.

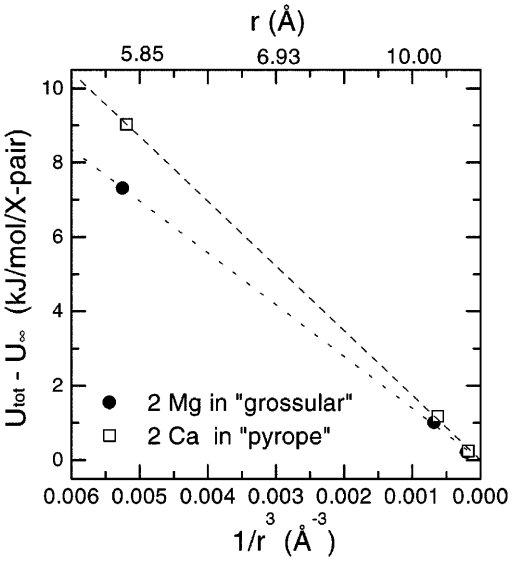

Fig. 6 Variation of total lattice energies (per pair of foreign atoms) of garnets with two foreign cations in a $3 \times 1 \times 1$ supercell as a function of the separation of the foreign dodecahedral cations in a tetrahedra-dodecahedra chain parallel [1 0 0]. U_∞ represents the lattice energy of the configuration with infinite separation between the foreign cations and was determined by linear regression

Interpretation of interaction energies in the dilute limit

In general, any distortion of coordination polyhedra is associated with changes in the total lattice energy. This basic knowledge provides an interpretation for the relative total lattice energies observed in the dilute limit. The analysis of the local structural environment around the foreign X cations (Mg in grossular-rich structure and Ca in pyrope-rich structure) showed that the neighbouring tetrahedra and octahedra are distorted relative to their geometries in the respective endmember structures. The distortions are greater the closer the polyhedra are to the foreign X cation. Using the model which describes the garnet structure as a three-dimensional $\{^{[6]}Al_2{}^{[4]}SiO_4\}^{6-}$ framework, one could expect that the underlying mechanism for accommodating different-sized divalent X site cations is a local tilting or rotation of rigid SiO_4 tetrahedra and AlO_6 octahedra. The garnet framework has, however, no degrees of freedom to allow for such localised motions. Like other structures consisting of edge-sharing octahedra, the garnet framework does not allow for rigid unit modes to occur (Hammonds et al. 1998). Therefore, any tilting or rotation of a tetrahedron or octahedron at any place in the framework to accommodate locally a different-sized dodecahedral cation requires all polyhedra in the framework to make exactly the same movement. For the long-range average of the garnet structure, X-ray diffraction methods have well documented the simultaneous effect of polyhedral rotation and deformation (e.g. Novak and Gibbs 1971; Geiger and Feenstra 1997). Apart from the fact that at least the Ca-bearing dodecahedral sites cannot take any shape but, because there is a minimum Ca-O bond length, have to remain large enough to accommodate the larger Ca cations, a collective distortion of all framework-building polyhedra would involve relatively large changes in the total lattice energy of the system. Much smaller changes in the total energy are needed, however, when only those tetrahedra and octahedra distort which are direct neighbours of the foreign X cation. As a result of the strong connectivity between the different polyhedra in the garnet structure, more distant-neighboured polyhedra are affected as well. Thereby, the amount of distortion decreases with increasing distance from the substituted site.

The cation exchange process in solid-solutions can be separated into: (1) a mechanical or strain-energy effect due to local distortion of the lattice; (2) a chemical effect, which results from an interaction (attraction or repulsion) between the atoms of neighbouring sites and (3) a Coulombic effect, when cations with different valences are interchanged (e.g. Swalin 1966). The first two effects will contribute to the total energy of pyrope-grossular garnets. Although the two effects cannot be completely separated, we can use this division to interpret the short-range interaction energies in garnets.

The substitution of a single foreign X site cation produces localized distortions, which give rise to a strain-energy term that contributes to the total lattice energy. When a second foreign X site cation is placed in the host structure, it will again cost a certain amount of energy. If the two foreign X site cations are so far away from each other that they do not interact, no chemical energy term has to be taken into account. This should be the case for configurations d6 and d7.

On the other hand, if the two foreign X site cations are close enough to interact with each other, an additional, repulsive energy term arises. This is the case for arrangement d3, where two like X cations occupy two dodecahedra that are corner-shared to the same tetrahedron. In the case where these are two big Ca cations in a pyrope host, the tetrahedron becomes compressed between the two dodecahedra, while in the case where the two foreign cations are Mg cations in a grossular host, the tetrahedron will be expanded. For arrangements d4 and d5, the repulsive energy term is smaller because of the larger interatomic distance between the two foreign X site cations in these arrangements.

According to their shorter interatomic distances, one could expect, therefore, that arrangements d1 and d2 have the largest interaction energies. However, exactly the opposite is the case. Their lower interaction energies can be interpreted as follows. Imagine, for example, placing a second foreign Ca cation in the part of the pyrope host-structure which has already been expanded and distorted by a first Ca cation. Instead of having to generate a completely new distorted and expanded environment, this second foreign Ca cation will only need to slightly enlarge the already distorted region around the first foreign Ca cation. The incorporation of the second cation in the vicinity of the first should therefore require a smaller "incorporation" energy term. Hence, if the smaller amount of strain energy needed to generate configurations d1 and d2 balances their repulsive energies, these arrangements can be energetically favourable.

Calculations in less dilute cases

Simulations for less dilute systems were made in $1 \times 1 \times 1$ supercells for garnet compositions where 3, 4, 6 and finally 12 Ca atoms were substituted for Mg on the 24 dodecahedral sites and vice versa. For the different compositions, random configurations of Ca and Mg cations on the dodecahedral sites were generated and the relative arrangements of like cation pairs were analyzed in terms of the number of the seven different pair interactions. These tasks were automated using the programming tools of Microsoft EXCEL. For the different garnet compositions the total lattice energies of the different configurations were finally analyzed in terms of the pair interaction by fitting the energies to the following model Hamiltonian:

$$E = E_0 + \sum_i n_i J_i \quad . \tag{4}$$

The ordering energy is given by

$$\Delta E^{ord} = \sum_i n_i J_i \ , \qquad (5)$$

where i denotes the type of pair interaction (first, second, third, ... or seventh-distant neighbour) and n_i are the number of Ca-Ca pairs (or Mg-Mg pairs for grossular-rich compositions) for the i-th interaction. In this manner, we obtained interaction energies, J_i, for the seven different interrelations between the dodecahedral sites. In Eq. (4), E_0 is an arbitrary energy chosen such that the J_1 value is 0 for all compositions. In this way the relative interaction energies for the different compositions can be directly compared. The J_i values obtained for the different compositions are listed in Table 6. Table 6 also contains further information on how many configurations were relaxed for every individual composition, what R value the fits to Eq. (4) resulted in, what the approximate distances between the different interacting sites are and how many of neighbours of each kind the different sites have. The J_i values are also presented graphically in Fig. 7. Some of the J values are in very good agreement with each other, while others show more differences. In the case of calculations with two and three foreign cations in a supercell, all possible configurations were calculated. This was not possible for less dilute compositions because of the large number of possible configurations. Hence, it is possible that the J values would be modified slightly if they were determined on the basis of other or more configurations. However, it can be concluded that the J values are barely dependent on the garnet composition.

The strongest repulsion of like cations is between dodecahedral sites that are linked via an edge-shared tetrahedron. In contrast to previous crystal-chemical solid-solution models such as the equivalent site model, we determined that it is not unfavourable to place large Ca cations next to each other in neighbouring edge-sharing dodecahedra. The quality of the fits of the interaction energies to the database of lattice energies indicates that the Hamiltonian given in Eq. (4) reasonably describes the dodecahedral cation interactions in garnet. This is illustrated in Fig. 8, which compares the total energies of the different configurations obtained from the GULP simulations with the energies calculated using Eq. (4) for the 50:50 mixture, i.e. Py50Gr50 composition.

We are confident that the values for the interaction constants J_i are reasonable, especially after our results for the simulations in the dilute limit were cross-checked with electronic structure calculation using the program SIESTA. The J values were found to be within 20% of the values determined.

Finally, it should be noted that in previous simulation studies, which investigated cation-ordering effects in minerals, pressure was not a matter of concern. This is because the calculations were undertaken at constant volume and/or the minerals studied were stable at room pressure. However, pyrope-grossular garnets are metastable at room pressures, and only thermodynamically stable at higher pressures. For example, pyrope and pyrope-rich garnets are only stable above 15 kbar (Boyd and England 1959). We tested, therefore, for the first time the influence of pressure on the interaction energies. This was done in a less rigorous study because it became rather quickly known that pressures of up to 100 kbar produce only minor variations in the interaction energies. Accordingly, we refrain from presenting these results in detail.

Monte Carlo methods

The simulation of the cation ordering process was performed using the Monte Carlo method. A pseudospin variable was assigned to each site, with value $\sigma = 1$ if

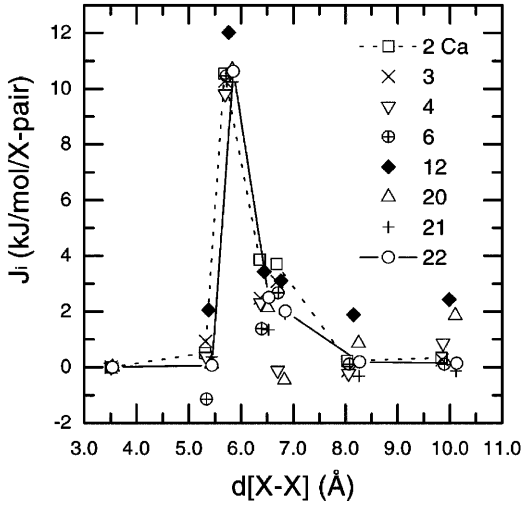

Fig. 7 Comparison of the interaction energies of the seven different types of dodecahedral neighbours for different numbers of Ca and Mg atoms in a $1 \times 1 \times 1$ supercell. The *numbers in the legend* refer to the number of Ca atoms per unit-cell and indicate the garnet composition

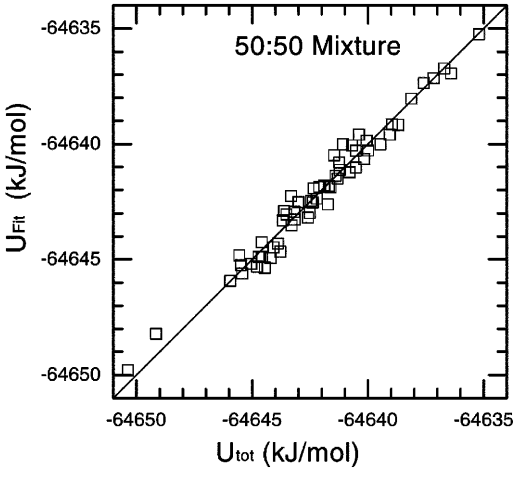

Fig. 8 Comparison of the observed modelled lattice energies of 60 random configuration with those calculated using Eq. (4) and the fitted J values of Table 6 for Py50Gr50

the site is occupied by one type of cation, and $\sigma = -1$ if occupied by the other type. Because the model is symmetric in composition, it actually is not relevant whether a positive value is assigned to occupancy by Mg or Ca. It can be shown (see, for example, Dove 1999) that within the J formalism given earlier, the Hamiltonian for an ensemble of interacting cations can be expressed in terms of the pseudospins as

$$\mathscr{H} = \frac{1}{4}\sum_{\langle j,k\rangle} J_{jk}\sigma_j\sigma_k \ , \tag{6}$$

where the sum is over all pairs of cation sites, j and k, avoiding counting each pair twice. Symmetrically related pairs of sites will, of course, have the same J values.

The Monte Carlo simulations were performed using the Ossia98 code on the Hitachi SR2201 parallel supercomputer of the Cambridge High-Performace Computing Facility (details are given in http://www.esc.cam.ac.uk/ossia). The simulations were based on the three dominant exchange energies (J_3, J_4 and J_5) and were performed in a $6 \times 6 \times 6$ supercell using periodic boundary conditions and repeated for many different temperatures. Analysis routines were used to calculate the probabilities of different first- and second-coordination shells consistent with those given by the NMR results during the progress of the Monte Carlo simulation at each temperature, and to average these over many configurations. The energy was recorded as a function of temperature in order to use it in the thermodynamic integration we now describe.

Derivation of thermodynamic functions by thermodynamic integration

The free energy, F, for a given model at a particular temperature, T, can be calculated in a Monte Carlo simulation using the method of thermodynamic integration. The starting point is to separate the model Hamiltonian, $\mathscr{H}$, into two parts

$$\mathscr{H} = \mathscr{H}_0 + \Delta\mathscr{H} \ , \tag{7}$$

where $\mathscr{H}_0$ is the Hamiltonian of a model that is similar to the model, but which can be solved exactly, and $\Delta\mathscr{H}$ is the remainder of the Hamiltonian. The free energy can be calculated from this separated Hamiltonian using a result that follows from the Bogoliubov inequality:

$$F = F_0 + \int_0^1 \langle\Delta\mathscr{H}\rangle_\lambda \mathrm{d}\lambda \ , \tag{8}$$

where F_0 is the free energy associated with the Hamiltonian $\mathscr{H}_0$. Conceptually, the tricky part is to obtain $\langle\Delta\mathscr{H}\rangle_\lambda$, which is the average of $(\mathscr{H} - \mathscr{H}_0)$ calculated from a distribution function for the system determined by the Hamiltonian

$$\mathscr{H}_\lambda = \lambda\mathscr{H} + (1-\lambda)\mathscr{H}_0 = \mathscr{H}_0 + \lambda\Delta\mathscr{H} \ , \tag{9}$$

where λ ranges in value from 0 to 1. In order to calculate $\langle\Delta\mathscr{H}\rangle_\lambda$, the distribution function can be obtained using a Monte Carlo simulation of the Hamiltonian $\mathscr{H}_\lambda$. That is, a simulation is performed using the Hamiltonian $\mathscr{H}_\lambda$, and the configuration of atoms generated by the simulation is used to calculate the energy $(\mathscr{H} - \mathscr{H}_0)$. For the simulation of order–disorder behaviour, the Hamiltonian $\mathscr{H}$ can be taken to represent a small perturbation of a system with random disorder, i.e. of a system with $\mathscr{H}_0 = 0$. Therefore, if the Hamiltonian is given by

$$\mathscr{H} = \frac{1}{4}\sum_{\langle j,k\rangle} J_{jk}\sigma_j\sigma_k \ , \tag{10}$$

it follows that

$$\mathscr{H}_\lambda = \frac{1}{4}\lambda\sum_{\langle j,k\rangle} J_{jk}\sigma_j\sigma_k \ . \tag{11}$$

The free energy is obtained by performing a set of simulations with the Hamiltonian $\mathscr{H}_\lambda$ at a fixed temperature but different values of λ, and to calculate the average $\langle\Delta\mathscr{H}\rangle_\lambda = \langle\mathscr{H}_\lambda\rangle/\lambda$ from the atomic configurations generated by the simulation. The integral is then performed by numerical integration of the results from the simulations performed over the range of values of λ.

In order to obtain the free energy as a function of temperature, $F(T)$, we note that a simulation performed at a temperature T using a Hamiltonian with the exchange constant ΛJ is equivalent to a simulation performed with the exchange constant J at a temperature T/Λ. Therefore, by varying the range of the integral in the equation above, we can obtain the free energy as a function of temperature. Formally, this procedure is represented by the equation

$$F(T/\Lambda) = \Lambda^{-1}F_0(T) + \int_0^\Lambda \langle\lambda\mathscr{H}\rangle_{T,\lambda}\mathrm{d}\lambda \ , \tag{12}$$

where $\Lambda < 1$, and the subscript T on the average $\langle\Delta\mathscr{H}\rangle_{T,\lambda}$ denotes that the average was obtained using a distribution obtained at the temperature T.

The free-energy function $F_0(T)$ in the calculation of the actual free energy corresponds to the free energy of a random distribution of two types of cations of proportion x and $(1-x)$ and is given by the usual result (expressed here as per atom):

$$F_0(T) = E_0 - TS_0 = k_\mathrm{B}T[x\ln x + (1-x)\ln(1-x)] \ . \tag{13}$$

Hence, we have

$$F_0(T/\Lambda) = \Lambda^{-1}F_0(T) \ . \tag{14}$$

This method has been used previously to calculate the free energy and entropy in simulations of the ordering of Al and Si atoms over the tetrahedral sites in the feldspar structure (Myers et al. 1998), where the focus was on the effects of having non-equal numbers of Al and Si atoms.

Monte Carlo results

In Figs. 9 and 10 we plot the Monte Carlo results for the ordering energy and configurational entropy for a number of solid-solution compositions. While the different mixtures cool down, their energies decrease according to the increasing avoidance of energetically unfavourable Mg-Mg and Ca-Ca third-nearest-neighbour pairs. For concentrations nearer Py50Gr50 these energy changes become larger, because the formation of Mg-Mg and Ca-Ca pairs is more easily avoidable. Although Fig. 9 shows clear evidence for increasing deviations from complete random disorder with decreasing temperature, no long-range order is formed in the different mixtures. This is because the third-nearest-neighbour sites, which correspond to the dominant interaction energy J3, are arranged along a linear chain of edge-sharing tetrahedra and dodecahedra. Hence, the interacting sites are arranged in a quasi one-dimensional structure which cannot have long-range order above 0 K (Dove et al. 1996). It is clear from the plots of Fig. 10 that all garnet compositions tend towards random disorder at high temperatures, as expected, and that at lower temperatures it is the samples with concentrations nearer 50% that depart most strongly from random mixing. This is in line with our earlier work on the role of changing concentration of two cation types on ordering phase transitions (Dove et al. 1996; Myers et al. 1998).

The interesting correlation is between the changes in entropy and the changes in the NMR spectra, although, as we will see, the correspondence between experiment and calculation is not good for some compositions. The ^{29}Si MAS NMR spectra show resonances for two-shell clusters of Mg and Ca surrounding the ^{29}Si nuclei. These clusters consist of two dodecahedral sites that are edge-shared to a SiO_4 tetrahedron (1st shell) and four dodecahedra that are corner-shared to the same tetrahedron (2nd shell). The first shell can be occupied by 2Mg0Ca, 1Mg1Ca or 0Mg2Ca and the 2nd shell

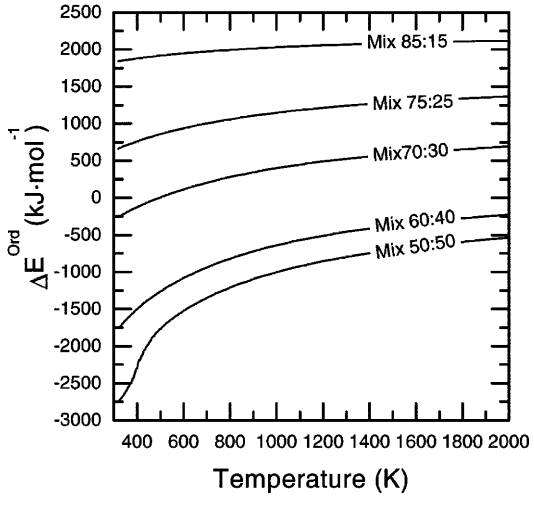

Fig. 9 Monte Carlo results of the ordering energy, $\Delta E^{\mathrm{ord}} = \frac{1}{4}\sum_{\langle ij \rangle} \sigma_i \sigma_j J_{ij}$, for a number of compositions

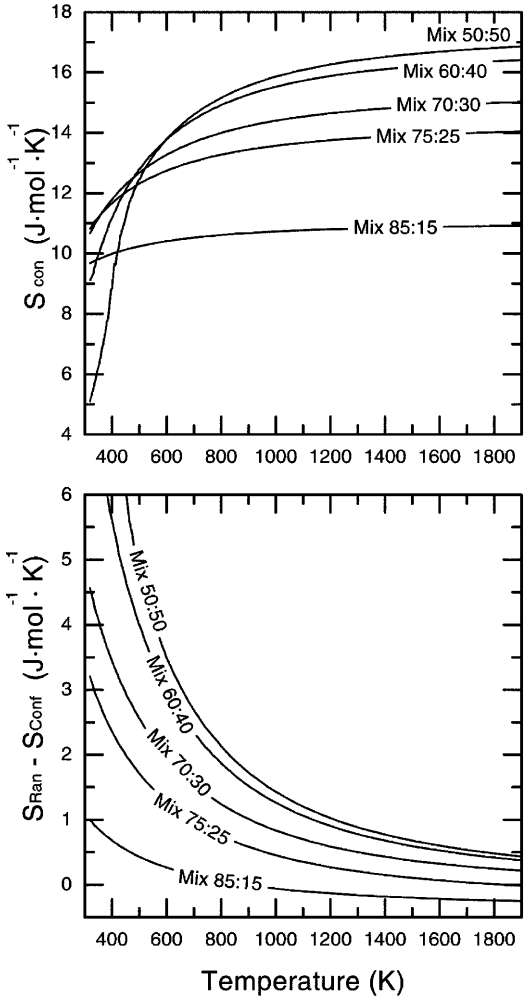

Fig. 10 Monte Carlo results of above configurational entropy for different compositions and below reductions of configurational entropy due to short-range ordering

by 4Mg0Ca, 3Mg1Ca, 2Mg2Ca, 1Mg3Ca or 0Mg4Ca. Hence, there are $3 \times 5 = 15$ different clusters. The intensity of any NMR resonance is proportional to the relative occupancy of the type of cluster to which it is assigned. In principle, the NMR spectra should show 15 resonance lines, but there is considerable overlap which means that assignments of the NMR lines to specific clusters cannot be done unambiguously. In addition, depending on garnet composition, some of the clusters have a very low occupancy and are not experimentally detectable. The cluster occupancies can readily be calculated in the Monte Carlo simulations, and these are shown for several compositions and as functions of temperature in Fig. 11. The clusters have been labelled according to the dominant cation in the first and second shell. For the pyrope-rich compositions, for example, in cluster 2, 4 all six dodecahedra are occupied by Mg cations and in cluster 1, 0 the 1st shell is occupied by one Mg and one Ca and the second shell by 0 Mg and 4 Ca cations, etc. We have indicated in Fig. 11 the data obtained from NMR experiments. In the case of Mix

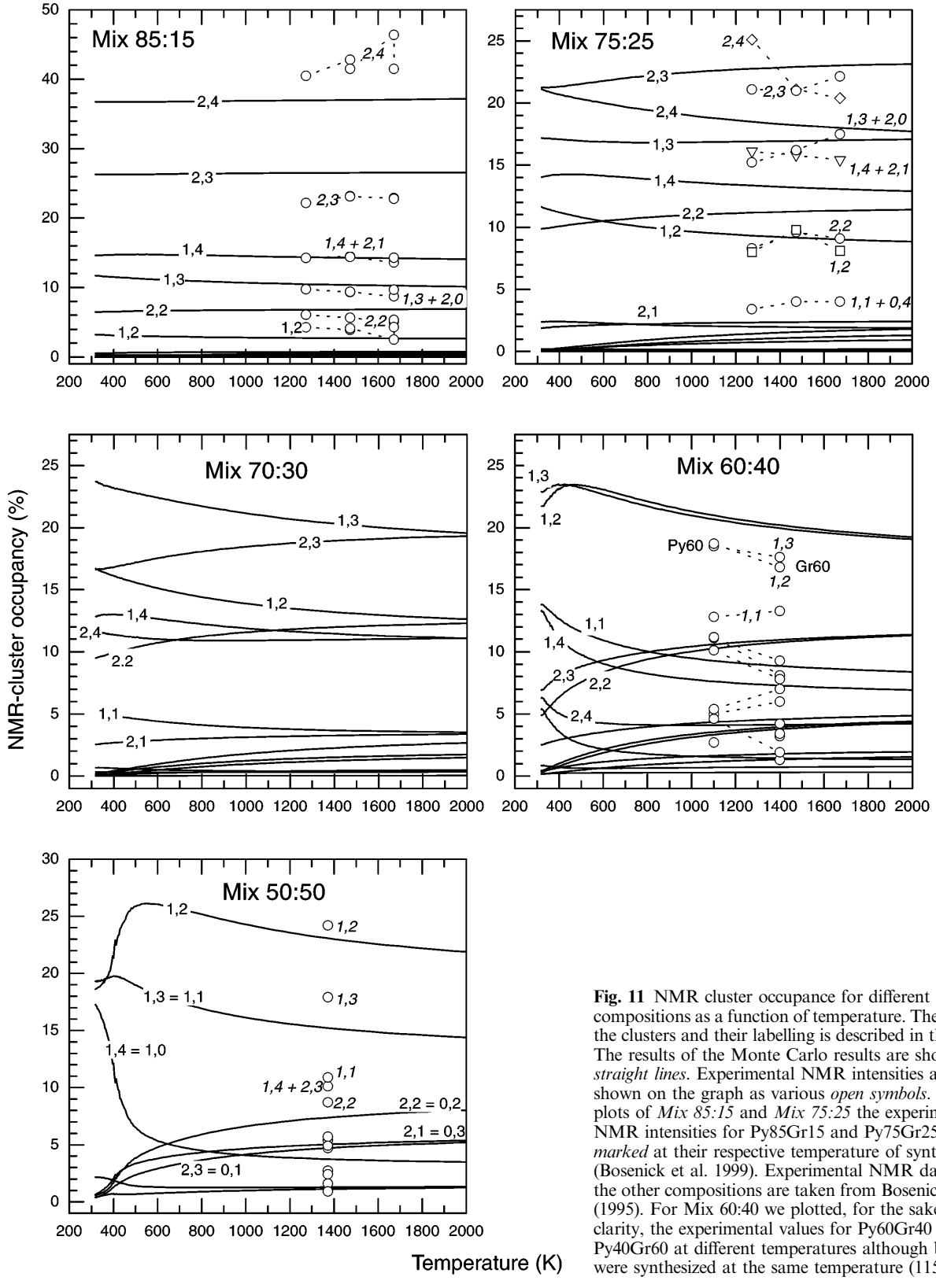

Fig. 11 NMR cluster occupance for different garnet compositions as a function of temperature. The size of the clusters and their labelling is described in the text. The results of the Monte Carlo results are shown as *straight lines*. Experimental NMR intensities are shown on the graph as various *open symbols*. On the plots of *Mix 85:15* and *Mix 75:25* the experimental NMR intensities for Py85Gr15 and Py75Gr25 are *marked* at their respective temperature of syntheses (Bosenick et al. 1999). Experimental NMR data for the other compositions are taken from Bosenick et al. (1995). For Mix 60:40 we plotted, for the sake of clarity, the experimental values for Py60Gr40 and Py40Gr60 at different temperatures although both were synthesized at the same temperature (1150 °C)

85:15 and Mix 75:25 we have indicated the experimental NMR line intensities of Py85Gr15 and Py75Gr25 at their different temperatures of synthesis (Bosenick et al. 1999). In the case of Mix 60:40 we have plotted the experimental results of Py60Gr40 at 1000 K and those of Gr60Py40 at 1300 K although both garnets were synthesized at 1323 K (Bosenick et al. 1995). In all cases, the cluster populations for a completely random

system are given by the results for high temperatures, and clearly some of the populations significantly depart from the random values on cooling.

The important aspects of the comparison between the calculated and observed NMR populations are in the extent to which they depart from their random values. Clearly, some clusters become more populated, and others less populated, on changing temperature, and the critical point is the extent to which the simulations can reflect the changes measured in the NMR experiment. In this regard, the simulations have mixed success. For the 15% composition, the simulations are consistent with the NMR result that there is little departure from the random structural state and very little variation with temperature. For the 25% composition the trends on lower synthesis temperature seen in the NMR spectra are in agreement with those of the simulations. For example, the occupancy of cluster 2, 4 increases, while that of cluster 2,3 decreases simultaneously. However, while for the lowest temperature of the experiment the intensity for cluster 2, 4 becomes larger than those of cluster 2, 3, this crossover is not predicted with the simulations.

In total, the correspondence between the NMR intensities and the experimental data is not as good as one might have hoped for, particularly when comparing with the differences between the cluster proportions at a specific temperature and at infinite temperature. Clearly, the occupancies of some clusters are reduced, and others are increased, on cooling, and the changes obtained in the Monte Carlo simulations are not always correlated with the occupancy derived from the NMR spectra. This may be due to inadequacies in the MC method (and in this respect we note that the MC simulations force a symmetry between Mg and Ca which may not be present in the data), or it may be that the overlapping of lines in the NMR spectra has led to unidentified systematic errors in the determination of line intensities. For example, in Py50Gr50, the clusters 1, 1 and 1, 3 should be identical according to symmetry, but in the experimental data the cluster 1, 3 has clearly a higher occupancy than 1, 1. On the other hand, in the 75:25 mix, the changes in the top four clusters are similar in the simulations and NMR data, although the absolute numbers are not a perfect match.

It is interesting to note that some of the cluster occupancies change significantly at low temperatures. For example, in the 50:50 mix, the 1, 2 cluster occupancy initially increases on cooling above that found in a random configuration, but suddenly at 600 K it drops down to below its random value. This effect is most prominent for the compositions near Py50Gr50, and is not seen in the 75:25 or 85:15 mixes. It is interesting, though, that this effect does not obviously show itself in the entropy. In fact, one can comment that changes in entropy are far more dramatic than changes in cluster occupancies. For example, if one considers the 70:30 mix, the largest change in the cluster occupancy on cooling from high temperatures is around 4% for the most significant clusters (this is an absolute value – at high temperatures the occupancy is around 50%). Yet the change in entropy on cooling to 400 K is around 30% of its value at high temperatures. This might suggest that NMR data are relatively insensitive to changes in entropy, implying that it could be very difficult to estimate entropy from NMR line intensities.

Acknowledgements This work was initiated as part of a priority program concerning element partitioning in rock-forming minerals, grant number Ge 649/2-3 of the Deutsche Forschungsgemeinschaft. It has also been supported by the National Environment Research Council (grant no. GR3/10606). The Monte Carlo simulations were performed on the Hitachi parallel computer of the Cambridge High Performance Computing Facility. The first author would like to gratefully acknowledge the award of a Marie Curie Research Fellowship by the European Community. Many thanks to T. Boffa Ballaran for her active support, data exchange and agile discussions about her HMIR study on garnets.

References

Armbruster T, Geiger CA (1993) Andradite crystal chemistry, dynamic X site disorder and structural strain in silicate garnets. Eur J Mineral 5: 59–71

Armbruster T, Geiger CA, Lager GA (1992) Single-crystal X-ray structure study of synthetic pyrope almandine garnets at 100 and 293 K. Am Mineral 77: 512–521

Berman RG (1990) Mixing properties of Ca-Mg-Fe-Mn garnets. Am Mineral 75: 328–344

Berman RG, Koziol AM (1991) Ternary excess properties of grossular-pyrope-almandine garnet and their influence in geothermobarometry. Am Mineral 76: 1223–1231

Bertram UC, Heine V, Jones IL, Price GD (1990) Computer modelling of Al/Si ordering in sillimanite. Phys Chem Miner 17: 326–333

Boffa Ballaran T, Carpenter MA, Geiger CA, Koziol AM (1999) Local structural heterogeneity in garnet solid solutions. Phys Chem Miner 26: 554–569

Boyd FR, England JL (1959) Pyrope. Carnegie Inst Wash, Yearbook 58: 83–87

Born L, Zemann J (1964) Abstandsrechnungen und gitterenergetische Berechnungen an Granaten. Contrib Mineral Petrol 10: 2–23

Bosenick A, Geiger CA (1997) Powder diffraction study of synthetic pyrope-grossular garnets between 20 and 295 K. J Geophys Res 102, B10: 22649–22657

Bosenick A, Geiger CA, Schaller T, Sebald A (1995) An ^{29}Si MAS NMR and IR spectroscopic investigation of synthetic pyrope-grossular garnet solid solutions. Am Mineral 80: 691–704

Bosenick A, Geiger CA, Phillips BL (1999) Local Ca-Mg distribution of Mg-rich pyrope-grossular garnets synthesized at different temperatures revealed by ^{29}Si MAS NMR spectroscopy. Am Mineral 84: 1423–1433

Bush TS, Gale JD, Catlow CRA, Battle PD (1994) Self-consistent interatomic potentials for the simulation of binary and ternary oxides. J Mater Chem 4: 831–837

Catlow CRA (1988) Computer modelling of silicates. In: Salje EKH (ed) Physical properties and thermodynamic behaviour of minerals. NATO ASI series C 225. Reidel, Boston, pp 619–638

Catlow CRA, Mackrodt JR, Stewart RF (1982) Defect energies in aluminium oxide and rutile titanium oxide. Phys Rev B 25: 1006–1026

Clark JR, Appleman DE, Papike JJ (1969) Crystal-chemical characterization of clinopyroxenes based on eight new structure refinements. Min Soc Am Mineral Spec Pap 2: 31–50

Dempsey MJ (1980) Evidence for structural changes in garnet caused by calcium substitution. Contrib Mineral Petrol 71: 281–282

Dove MT (1989) On the computer modeling of diopside: toward a transferable potential for silicate minerals. Am Mineral 74: 774–779

Dove MT (1999) Order/disorder phenomena in minerals: ordering phase transitions and solid solutions. In: Wright K, Catlow CRA (eds) Microscopic properties and processes in minerals. NATO ASI series C, 543. Kluwer, Dordrecht, pp 451–475

Dove MT, Cool T, Putnis A, Salje EKH, Winkler B (1993) On the role of Al-Si ordering in the cubic-tetragonal phase transition of leucite. Am Mineral 78: 486–492

Dove MT, Thayaparam S, Heine V, Hammonds KD (1996) The phenomenon of low Al-Si ordering temperatures in aluminosilicate framework. Am Mineral 81: 349–362

Gale JD (1997) GULP – a computer program for the symmetry adapted simulation of solids. JCS Faraday Trans 93: 629–637

Ganguly J, Cheng W, O'Neill HStC (1993) Syntheses, volume, and structural changes of garnets in the pyrope-grossular join: implications for stability and mixing properties. Am Mineral 78: 583–593

Gavrieli I, Matthews A, Holland TJB (1996) Ca-Mn exchange between grossular and $MnCl_2$ solutions at 2 kbar and 600 °C: reaction mechanism and evidence for non-ideal mixing in spessartine-grossular garnets. Contrib Mineral Petrol 125: 251–262

Geiger CA (1999) Thermodynamics of $(Fe^{2+}, Mn^{2+}, Mg, Ca)_3Al_2Si_3O_{12}$ garnet: a review and analysis. Mineral Petrol 66: 271–299

Geiger CA, Armbruster T (1997) $Mn_3Al_2Si_3O_{12}$-spessartine and $Ca_3Al_2Si_3O_{12}$-grossular garnet: structural dynamic and thermodynamic properties. Am Mineral 82: 740–747

Geiger CA, Feenstra A (1997) Molar volumes of mixing of almandine-pyrope and almandine-spessartine garnets and the crystal chemistry and thermodynamic-mixing properties of the aluminosilicate garnets. Am Mineral 82: 571–581

Geiger CA, Rossmann GR (1994) Crystal field stabilization energies of almandine-pyrope and almandine-spessartine garnets determined by FTIR near infrared measurements. Phys Chem Miner 21: 516–525

Geiger CA, Newton RC, Kleppa OJ (1987) Enthalpy of mixing of synthetic almandine-grossular and almandine-pyrope garnets from high-temperature solution calorimetry. Geochim Cosmochim Acta 51: 1755–1763

Geiger CA, Armbruster T, Lager GA, Jiang K, Lottermoser W, Amthauer G (1992) A combined temperature-dependent ^{57}Fe Mössbauer and single crystal X-ray diffraction study of synthetic almandine: evidence for the Gol'danskii-Karyagin effect. Phys Chem Miner 19: 121–126

Hammonds KD, Bosenick A, Dove MT, Heine V (1998) Rigid unit modes in crystal structures with octahedrally coordinated atoms. Am Mineral 83: 476–479

Haselton HT, Westrum EJ (1980) Low-temperature heat capacities of synthetic pyrope, grossular and pyrope60grossular40. Geochim Cosmochim Acta 44: 701–709

Hazen RM, Finger LW (1978) Crystal structures and compressibilities of pyrope and grossular to 60 kbar. Am Mineral 63: 297–303

Levien L, Wiedner DJ, Prewitt CT (1979) Elasticity of diopside. Phys Chem Miner 4: 105–133

Lewis GV (1984) Computer modelling of mixed oxides. PhD Thesis, University of London

Meagher EP (1975) The crystal structures of pyrope and grossularite at elevated temperatures. Am Mineral 60: 218–228

Meagher EP (1980) Silicate garnets. In: Ribbe PH (ed) Orthosilicates. Rev Mineral 5: 25–66

Menzer G (1928) Die Kristallstruktur der Granate. Z Krist 69: 300–396

Merli M, Callegari A, Cannillo E, Caucia F, Leona M, Oberti R, Ungaretti L (1995) Crystal chemical complexity in natural garnets: structural constraints on chemical variablility. Eur J Mineral 6: 1239–1250

Myers ER, Heine V, Dove MT (1998) Thermodynamics of Al/Al avoidance in the ordering of Al/Si tetrahedral framework structures. Phys Chem Miner 25: 457–464

Newton RC, Wood BJ (1980) Volume behavior of silicate solid solutions. Am Mineral 65: 733–745

Newton RC, Charlu TV, Kleppa KM (1977) Thermochemistry of high pressure garnets and clinopyroxenes in the system CaO-MgO-Al_2O_3-SiO_2. Geochim Cosmochim Acta 41: 369–377

Novak GA, Gibbs GV (1971) The crystal chemistry of silicate garnets. Am Mineral 56: 791–825

Nuber B, Schmetzer K (1982) Über systematisch ausgelöschte Reflexe im Beugungsbild eines natürlichen Granat-Mischkristalls. Naturwissenschaften 69: 141

Post JE, Burnham CW (1986) Ionic modeling of mineral structures and energies in the electron gas approximation: TiO_2 polymorphs, quartz, forsterite, diopside. Am Mineral 71: 142–150

Price GD, Parker SC (1988) The computer simulation of the lattice dynamics of silicates. In: Salje EKH (ed) Physical properties and thermodynamic behaviour of minerals. NATO ASI Series C, 225. Riedel, Boston, pp 591–618

Price GD, Parker SC, Leslie M (1987) The lattice dynamics and thermodynamcis of the Mg_2SiO_4 polymorphs. Phys Chem Miner 15: 181–190

Putnis A, Vinograd V (1999) Principles of solid state NMR spectroscopy and applicaions to determining local order in minerals. In: Wright K, Catlow CRA (eds) Microscopic processes in minerals. NATO ASI series C, 543. Kluwer, Dordrecht, pp 389–425

Quartieri S, Chaboy J, Merli M, Oberti R, Ungaretti L (1995) Local structural environment of calcium in garnets – a combined structure refinement and XANES investigation. Phys Chem Miner 22: 159–169

Quartieri S, Antonioli G, Geiger CA, Artioli G, Lottici PP (1999) XAFS characterization of the structural site of Yb in synthetic pyrope and grossular garnets. Phys Chem Minerals 26: 251–256

Renner B, Lehman G (1986) Correlation of angular and bond length distortion in TiO_4-units in crystals. Z Krist 175: 43–59

Robinson K, Gibbs GV, Ribbe PH (1971) Quadratic elongation: a quantitative measure of distortion in coordination polyhedra. Science 172: 567–570

Rossmanith E, Armbruster T (1995) The intensity of forbidden reflections of pyrope: Umweganregung or symmetry reduction? Z Kristallogr, 210, 645–649

Sanders MJ, Leslie M, Catlow CRA (1984) Interatomic potentials for SiO_2. J Chem Soc, Chemical Communications 19: 1271–1273

Sangster MJL, Stoneham AM (1981) Calculations of off-center displacements of divalent substitutional ions in Cao, SrO and BaO from model potentials. Philos Mag B – Electron Opt Magnet Properties 43: 597–608

Swainson IP, Dove MT, Schmahl WW, Putnis A (1992) Neutron powder diffraction study of the akermanite-gehlenite solid solution series. Phys Chem Miner 19: 185–195

Swalin RA (1966) Thermodynamics of solids. John Wiley, New York

Thayaparam S, Dove MT, Heine V (1994) A computer simulation study of Al/Si ordering in gehlenite and the paradox of the low transition temperature. Phys Chem Miner 21: 110–116

Thayaparam S, Dove MT, Heine V, Hammonds KD (1996) A computational study of Al/Si ordering in cordierite. Phys Chem Miner 23: 127–139

Ungaretti L, Leona M, Merli M, Oberti R (1995) Non-ideal solid-solution in garnet: crystal-structure evidence and modelling. Eur J Mineral 7: 1301–1312

Winkler B, Dove MT, Leslie M (1991) Static lattice energy minimization and lattice dynamics calculations on aluminosilicate minerals. Am Mineral 76: 313–331

Zemann A (1962) Zur Kristallchemie der Granate. Beitr Mineral Petrol 8: 180–188

Zhang L, Ahsbahs H, Kutoglu A (1998) Hydrostatic compression and crystal structure of pyrope to 33 Gpa. Phys Chem Miner 25: 301–307

Appendix

Since the Ca potential, Ca-3, of Bush et al. (1994) has not been previously used in simulation studies on minerals, we tested its transferability by calculating the structures of diopside and

Table 7 Comparison of cell dimension and atomic coordinates of the diopside structure calculated using different Ca···O-potentials with experimentally determined values. (Clark et al. 1969)

	Observed	Calculated		
		Ca-1	Ca-2	Ca-3
a (Å)	9.746	9.572	9.649	9.678
b (Å)	8.899	8.693	8.957	8.862
c (Å)	5.251	5.170	5.164	5.212
β (°)	105.63	104.62	104.02	105.17
Si				
x	0.2862	0.2858	0.2821	0.2839
y	0.0933	0.0971	0.0955	0.0951
z	0.2293	0.2306	0.2073	0.2206
O1				
x	0.1156	0.1140	0.1125	0.1132
y	0.0873	0.0945	0.0872	0.0902
z	0.1422	0.1437	0.1383	0.1404
O1				
x	0.3611	0.3598	0.3541	0.3572
y	0.2500	0.2550	0.2505	0.2516
z	0.3180	0.3260	0.2918	0.3072
O2				
x	0.3505	0.3574	0.3535	0.3534
y	0.0176	0.0185	0.0155	0.0143
z	0.9953	0.9965	0.9752	0.9919
Mg				
x	0.0000	0.0000	0.0000	0.0000
y	0.9082	0.9071	0.9062	0.9057
z	0.2500	0.2500	0.2500	0.2500
Ca				
x	0.0000	0.0000	0.0000	0.0000
y	0.3015	0.3030	0.3073	0.2990
z	0.2500	0.2500	0.2500	0.2500

Table 8 Comparison of the bond lengths and bond angles within the diopside structure calculated using different Ca···O-potentials with experimental data determined by Clark et al. (1969)

	Observed	Calculated		
		Ca-1	Ca-2	Ca-3
Si-O(1)	1.602	1.591	1.589	1.595
Si-O(2)	1.585	1.566	1.567	1.570
Si-O(3)	1.664	1.679	1.680	1.675
Si-O(4)	1.687	1.700	1.707	1.701
Mean	1.635	1.634	1.636	1.635
O(1)-Si-O(2)	118.2	118.0	118.7	118.1
O(1)-Si-O(3)	110.3	112.4	112.0	112.2
O(1)-Si-O(4)	109.9	110.7	110.3	109.4
O(2)-Si-O(3)	109.7	108.6	107.7	108.5
O(2)-Si-O(4)	103.6	103.6	103.6	102.8
O(3)-Si-O(4)	104.0	102.2	102.7	104.4
Mg-O(1)	2.16	2.10	2.10	2.12
Mg-O(2)	2.06	2.05	2.02	2.04
Mg-O(3)	2.05	1.99	2.03	2.01
Mean	2.08	2.05	2.05	2.06
Ca-O(1)	2.36	2.25	2.38	2.29
Ca-O(2)	2.35	2.31	2.49	2.40
Ca-O(3)	2.56	2.48	2.55	2.54
Ca-O(4)	2.72	2.60	2.58	2.69
Mean	2.50	2.41	2.50	2.48

Table 9 Comparison of the elastic constants (Mbar) of diopside calculated using different Ca···O potentials with experimental data. (Levien et al. 1979)

	Observed	Calculated		
		Ca-1	Ca-2	Ca-3
c11	2.23	2.38	2.48	2.19
c22	1.71	1.96	2.29	1.88
c33	2.35	3.30	3.01	3.06
c44	0.74	0.70	0.77	0.70
c55	0.67	0.55	0.75	0.57
c66	0.66	0.86	1.04	0.78
c12	0.77	1.11	1.20	1.03
c13	0.81	0.83	0.97	0.82
c23	0.57	0.83	0.87	0.77
c15	0.17	0.32	0.17	0.25
c25	0.07	0.17	−0.02	0.10
c35	0.43	0.45	0.33	0.38
c46	0.07	0.15	−0.07	0.10

Table 10 Comparison of the crystal structure of gehlenite calculated using different Ca···O potentials with experimental data (Swainson et al. 1992). T(1) is occupied by equal numbers of Al and Si atoms. To model this site an effective potential was used in the calculation. (see Winkler et al. 1991)

	Observed	Calculated		
		Ca-1	Ca-2	Ca-3
a (Å)	7.685	7.592	7.700	7.679
c (Å)	5.064	4.896	5.090	5.061
Ca				
x	0.339	0.341	0.339	0.338
y	0.161	0.159	0.161	0.162
z	0.510	0.517	0.512	0.514
T(1)*				
x	0.143	0.143	0.141	0.142
y	0.357	0.357	0.359	0.358
z	0.954	0.957	0.962	0.961
Al				
x	0	0	0	0
y	0	0	0	0
z	0	0	0	0
O(1)				
x	0.5	0.5	0.5	0.5
y	0	0	0	0
z	0.177	0.196	0.176	0.181
O(2)				
x	0.143	0.141	0.141	0.142
y	0.357	0.359	0.359	0.358
z	0.284	0.300	0.287	0.288
O(3)				
x	0.088	0.093	0.087	0.091
y	0.168	0.165	0.170	0.167
z	0.808	0.795	0.811	0.810

gehlenite. The structure of diopside has been a challenging task for modelling (Dove et al. 1989) and, hence, is a good test phase. Tables 7–10 compare the results obtained with the three different Ca potentials and experimental data. In the case of diopside it is not possible to decide whether the modified Ca potential (Ca-2) or the commonly used potential (Ca-1) gives a better representation of the structure. When comparing the elastic constants of diopside, the latter is superior because the modified potential gives negative values for some of the constants. On the other hand, the results for the gehlenite structure are better with the modified potential Ca-2. However, the Ca potential, Ca-3, that models the grossular structure best also gives the best model for diopside and gehlenite. This is evident from a simple comparison of the unit-cell parameters. In addition, for diopside the bond lengths and angles and the elastic constants are always closer to experimental values than those calculated using one of the other Ca potentials. Hence, the Ca potential, Ca-3, of Bush et al. (1994) is not only transferable to other minerals, but it also gives better results than the potential of Post and Burnham (1986), at least in the case of garnet, diopside and gehlenite.